2016

Characterization of Mechanical Properties of Gamma Irradiated Additively Manufactured Articles for In-Space Manufacturing

Behzad Rankouhi
South Dakota State University

CHARACTERIZATION OF MECHANICAL PROPERTIES OF GAMMA IRRADIATED ADDITIVELY MANUFACTURED ARTICLES FOR IN-SPACE MANUFACTURING

BY

BEHZAD RANKOUHI

A thesis submitted in partial fulfillment of the requirements for the

Master of Science

Major in Mechanical Engineering

South Dakota State University

2016

CHARACTERIZATION OF MECHANICAL PROPERTIES OF GAMMA IRRADIATED ADDITIVELY MANUFACTURED ARTICLES FOR IN-SPACE MANUFACTURING

This thesis is approved as a creditable and independent investigation by a candidate for the Master of Science in Mechanical Engineering degree and is acceptable for meeting the dissertation requirements for this degree. Acceptance of this does not imply that the conclusions reached by the candidates are necessarily the conclusions of the major department.

Todd Letcher, Ph.D.
Thesis Advisor Date

Fereidoon Delfanian, Ph.D.
Major Advisor Date

Kurt Bassett, Ph.D.
Head, Mechanical Engineering Department Date

Dean, Graduate School Date

ACKNOWLEDGEMENTS

I wish to sincerely thank my thesis advisor Dr. Todd Letcher for his valuable suggestions throughout the process of completing this project, for believing in me and for his trust. I also owe a debt of gratitude to my major advisor Dr. Fereidoon Delfanian for providing access to METLAB and its state of the art equipment, for his precious mentorship and continuous support during the past two years. Besides my advisors, I would also like to thank Dr. Robert McTaggart for his consultation on radiation physics and nuclear engineering side of this work. Without they precious support it would not be possible to conduct this research.

CONTENTS

ABBREVIATIONS

ABS	Acrylonitrile Butadiene Styrene
AM	Additive Manufacturing
ANOVA	Analysis Of Variance
ASTM	American Society for Testing and Materials
CF-ABS	Carbon Fiber reinforced ABS
CME	Coronal Mass Ejections
DMLS	Direct Metal Laser Sintering
FDM	Fused Deposition Modeling
GCR	Galactic Cosmic Rays
ISS	International Space Station
LEO	Low Earth Orbit
PEEK	Polyether Ether Ketone
PEI	Polyetherimide
PLA	Polylactic Acid

LIST OF FIGURES

CHAPTER 1

CHAPTER 2

LIST OF TABLES

CHAPTER 1

CHAPTER 2

ABSTRACT

CHARACTERIZATION OF MECHANICAL PROPERTIES OF GAMMA IRRADIATED ADDITIVELY MANUFACTURED ARTICLES FOR IN-SPACE MANUFACTURING

BEHZAD RANKOUHI

2016

Recently, additive manufacturing (AM) has opened many doors to engineers across various industries, such as medical, bio-engineering, automotive and recently, aerospace. In an effort to contribute to the development of AM in aerospace industry, a series of experiments were designed to help understand the behavior of 3D printed parts and extend its capabilities and possible uses. The first chapter of this project will focus on understanding the mechanical behavior of additively manufactured articles. In this chapter, a comprehensive effort was undertaken to represent the strength of a 3D printed object as a function of layer thickness by investigating the correlation between the mechanical properties of 3D printed parts and layer thickness. Results showed that samples printed with 0.2 mm layer thickness exhibit higher elastic modulus, ultimate strength and force compared with 0.4 mm. This result has a direct effect on decision making and future use of 3D printing; particularly functional load bearing parts.

The second chapter is focused on the effects of gamma irradiation on mechanical properties of hybrid materials as an in-space 3D printing feedstock to investigate the forthcoming possibilities of this technology for future space exploration missions. 3D printed testing samples were irradiated at different dosages from 1 to 1400 kGy using a Cobalt-60 gamma irradiator to simulate space radiation environment. The correlation between the mechanical properties of irradiated samples and accumulated radiation dosage were evaluated by a series of tensile and flexural tests. Findings showed a significant decrease in mechanical performance and noticeable changes in appearance of the parts with accumulated dosage of 1000 kGy and higher. However, for dosages below 10 kGy, samples showed no significant decrease in mechanical performance or change in appearance. These results were used to predict the life of a 3D printed part and demonstrate their potential for use on board the international space station, on low earth orbit satellites, in deep space and long duration missions.

CHAPTER 1

FAILURE ANALYSIS AND MECHANICAL CHARACTERIZATION OF 3D PRINTED ABS WITH RESPECT TO LAYER THICKNESS AND ORIENTATION

INTRODUCTION

Complex geometries have always been out of reach for designers and manufacturers until the advent of additive manufacturing (AM) in the 1980s. ASTM defines the process as the "process of joining materials to make objects from three-dimensional (3D) model data, usually layer upon layer, as opposed to subtractive manufacturing methodologies" [1]. AM is a very broad term which encompasses numerous methods such as binder jetting, direct metal laser sintering (DMLS®), fused deposition modeling (FDM), powder bed fusion and stereolithography. The FDM technique is of particular interest due to its association with desktop 3D printers. The term 3D printing is often used synonymously with AM, but is more commonly associated with machines that are low end in price and/or overall capability [1] and it usually refers to polymers and non-metal materials. The emergence of this term in the early 2010s made the technology popular among engineers and mainstream in public. This popularity has led the technology to become one of the fastest growing technologies in the world [2].

The FDM process works as follows: a thermo plastic polymer in form of a filament is extruded through a moveable nozzle head where it is deposited as a thread of molten material (raster) on a substrate (bed), usually made of glass or aluminum. Threads then solidify to form a layer of material. Additional layers are then deposited on top of each other to form a 3D object. So far, FDM has been mainly used in demonstrations, presentation models, visual aids and education which includes almost 25% of customer use in the AM industry [3]. Efforts have been undertaken during the past few years to prepare FDM to enter the realm of functional components which accounts for includes 29% of customer use (Fig. 1), [3]. The foremost obstacle facing to this transition is the

limited knowledge regarding the mechanical properties of printed parts. When it comes to functionality, structural integrity is of the highest importance. In order to achieve a desirable strength, the manufacturing process and, in turn, the final product properties need to be standardized. Lack of standards for FDM manufacturing and testing has led to incongruent conclusions of test results and print settings. For example, tensile properties of Acrylonitrile Butadiene Styrene (ABS) material manufactured using FDM has been reported to be between 11 MPa and 40 MPa [4-8]. This divergence can be partially explained by taking the anisotropic nature of printed parts into account [8]. Another impediment is the large number of influential variables in the FDM process (Fig. 2). Controlling all of these parameters is a perplexing task especially when there are no standards available for reference.

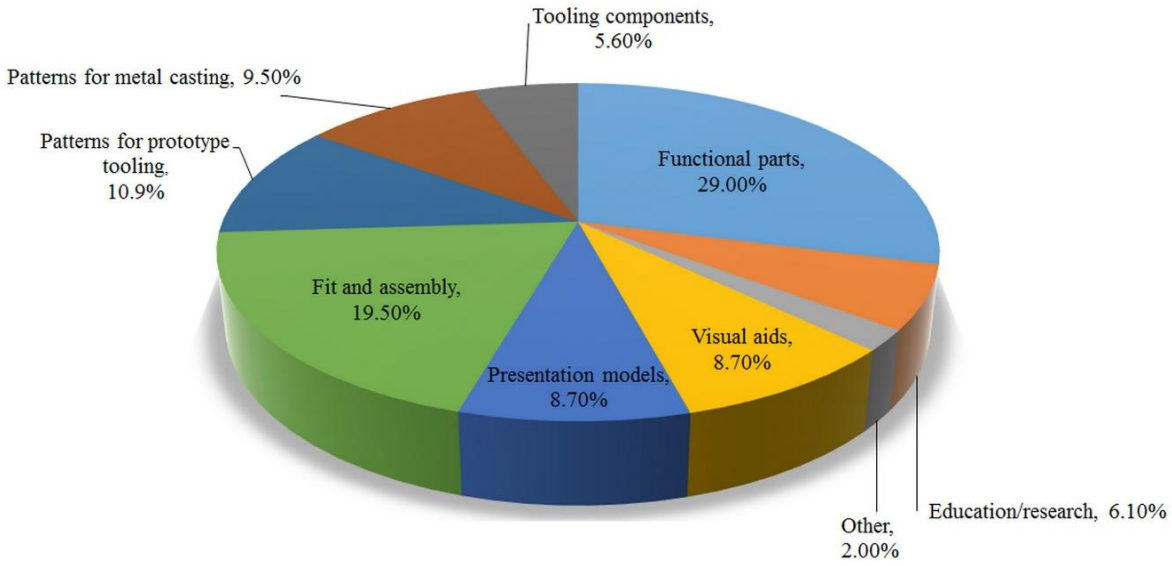

Fig. 1. Organizations' use of industrial AM systems for a range of applications [3].

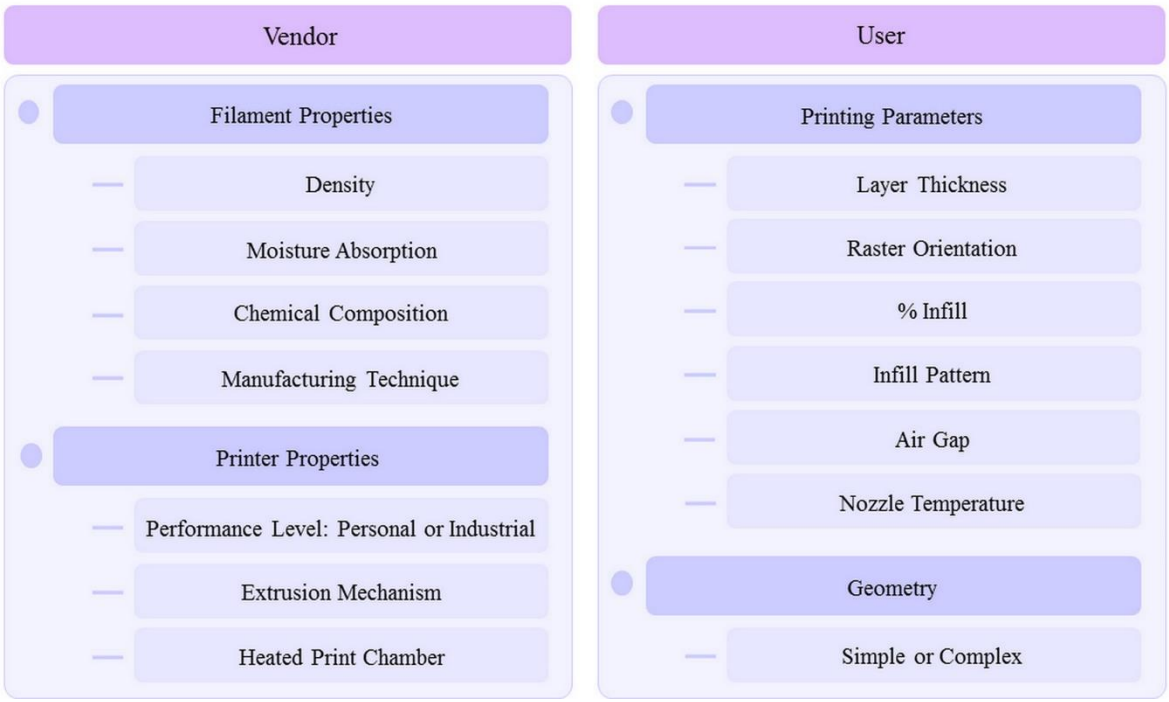

Fig. 2. Influential parameters on mechanical properties of parts fabricated using FDM.

Some work has been done to optimize some of these parameters for strength and design. Rodriguez et al. [9] utilized an integrated process-materials-design methodology to optimize the mechanical properties of parts fabricated using FDM for raster orientation aimed at moving FDM into volume production and functional components domain. Kara et al. [10] took a different approach in addressing the same problem. They used a surrogate-based optimization technique to improve load-carrying capacities of 3D printed parts by finding the optimum build orientation. Khan et al. [11] attempted to optimize different printing parameters, such as layer thickness, raster angle, and air gap size, to achieve maximum flexibility of the final part. Furthermore, effects of raster orientation on mechanical properties of parts fabricated using FDM have been extensively studied [2,

4, 7, and 8]. All agree that the strongest printing orientation is always along the pull direction.

A more controversial parameter is the layer thickness. Khan et al. [11] concluded that the optimal set of parameters for maximum performance of their model always include the smallest layer thickness (0.178 mm), while Sood et al. [12] stated that the tensile strength of their samples first decreased and then increased as the layer thickness increased. They associated the partial increase in strength with stronger diffusion between adjacent rasters due to high temperature gradients. They also hypothesized that the decrease in strength is due to the large number of heating and cooling cycles and the consequent residual stresses that follow. On the other hand Tymark et al. [4] inferred that samples with the largest layer thickness showed higher elastic modulus and samples with the lowest layer thickness had the highest tensile strength. Ahn et al. [8] deduced a low level of significance for effects of layer thickness on tensile strength of ABS specimens. Moreover, Anitha et al. [13] reported 51.57% effectiveness at 99% level of significance for effects of layer thickness on surface roughness of components produced using FDM. Effects of layer thickness have been studied in other forms of 3D printing processes as well [14]. None of the aforementioned studies have thoroughly investigated the effects of layer thickness. The inconsistency in reported results is another indication that effects of printing parameters on mechanical properties of parts still need to be studied, particularly in regards to layer thickness.

The use of FDM machines for manufacturing functional parts is rapidly growing, especially in fields of biomedical and robotic engineering [15-20] and is transitioning from a do-it- yourself hobbyist machine into a more robust and reliable manufacturing

system. To help expedite this transition, a comprehensive knowledge of the influential parameters on mechanical properties of manufactured parts is required. The work presented in this paper attempts to address the debatable layer thickness effects on the mechanical properties of 3D printed ABS samples using FDM through a set of extensive tensile tests followed by statistical analysis of the results. It is an extension of a preliminary study by Letcher et al. [2]. In addition, a failure analysis is presented via microscopic inspection of fracture areas and air-gap measurements. The practicality of results was further demonstrated by testing a typical A-Frame as a case example. The proposed findings can help designers and manufacturers to better understand the effects of print parameters on their components and make engineering decisions by evaluating time, material usage and strength of the final product.

EXPERIMENTAL SETUP

The goal of this study was to investigate the correlation between layer thickness and mechanical properties of additively manufactured parts using FDM. In order to do so, mechanical tensile tests were performed on samples made of ABS, one of the most common materials used for FDM process. ABS is a thermoplastic polymer, a material which becomes moldable at a relatively low glass transition temperature and solidifies upon cooling. Other prevalent thermoplastic polymers used in FDM process are Polylactic Acid (PLA), Polyether Ether Ketone (PEEK), ULTEM which is an amorphous thermoplastic polyetherimide (PEI) material, nylon and polycarbonate (PC).

The first step in designing the experiment was choosing the geometry of the specimens. There are no specific standard test methods available for parts fabricated

using FDM. ASTM D638 [21] is the best available choice for preparing samples; however, there have been reports of premature failure of 3D printed parts during testing due to accumulated stress concentration at fillet areas [2, 5, 6 and 8]. This stress concentration is mainly caused by raster termination near the fillet radius as shown by arrows in Figure 3. Increasing the number of layers can help alleviate the effects of this stress concentration by gradually filling the gaps as each layer deposits on top of the other. But thin samples, specimens that are made of a single or only a few layers, will still be affected by the discretization of rasters at fillets. To alleviate this issue, ASTM D3039 [22] guidelines were used to prepare the tensile testing samples (Fig. 4).

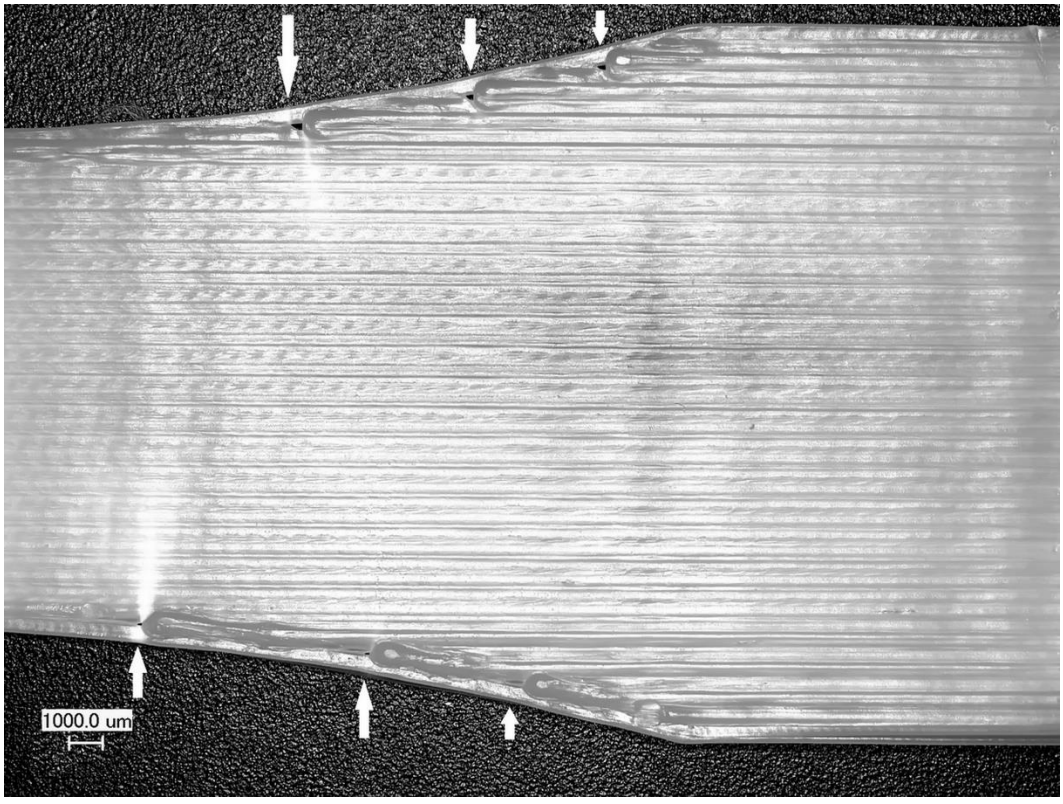

Fig. 3. Stress concentration due to raster discretization at fillet radius of a 0°, ASTM D638 sample.

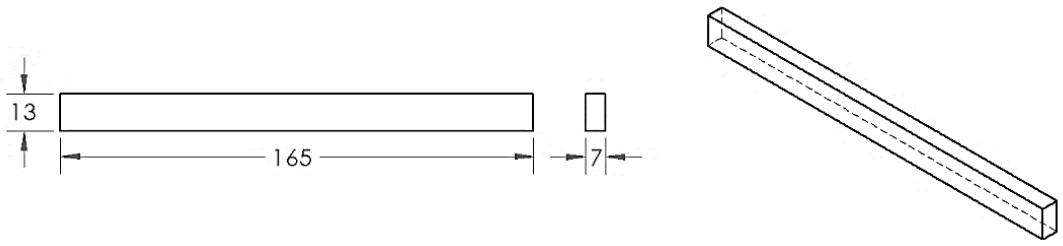

Fig. 4. Tensile test specimen with its dimensions in mm.

According to this standard, “design of mechanical test coupons remains to a large extent an art rather than a science, with no industry consensus on how to approach the engineering of the gripping interface.” This statement can be extended to parts manufactured by FDM process as well and is an indication of the anisotropic effects of these parts on their mechanical properties. Samples were printed using entry level 3D printer Makerbot Replicator 2x. Custom print profiles were created in to allow the printer to build samples with a single raster orientation throughout. Figure 5 depicts the orientations used with respect to pulling direction. To minimize the effects of uncontrolled parameters on the mechanical properties of printed parts, each sample was printed individually at the exact same position on the bed. A single perimeter was used for all samples to reduce its strengthening effects as reported by Croccolo et al. [6]. All samples were printed at 100% density. Using maximum infill can cause raster overlap or negative air-gap size, which, in turn, influences on the strength of the material [2]. The effects of air-gap size will be investigated in the results and discussion section of this paper. In this study, default settings were used on Makerware® software and raster overlapping was not a controlled variable throughout testing. All specimens were printed using the same generic brand of ABS filament.

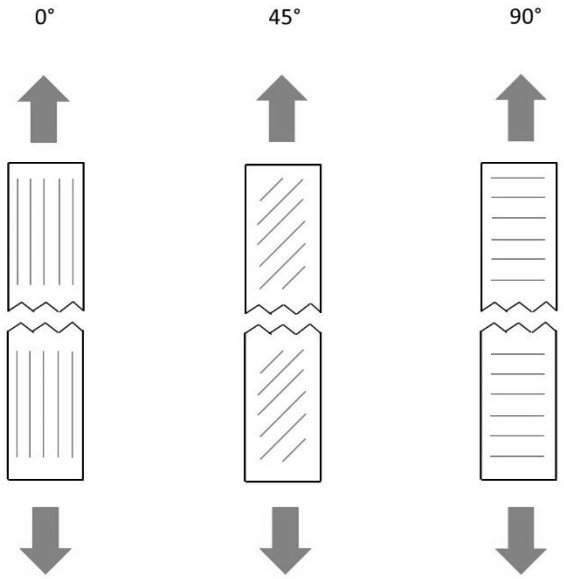

Fig. 5. Printed raster orientation with respect to pulling direction.

For comparison purposes, controlled printing parameters are tabulated in Table 1. Two nominal layer thicknesses were considered in this study, 0.2 and 0.4 mm. The thinnest samples have only one layer with nominal thickness of 0.2 and 0.4 mm. The thickest samples have 35 layers and 7 mm nominal thickness and 18 layers and nominal thickness of 7.2 mm for 0.2 and 0.4 mm treatments, respectively. Actual thickness and width were individually measured for each specimen using a caliper and minimum dimensions were used for performing calculations according to testing standards. A total of 372 samples were tested in this study. Four samples were tested for each layer number. Table 2 shows details of samples used as tensile test specimens in this study.

Tests were conducted using an MTS Insight 5 system with a 5 kN load cell. Built-in LVDTs measured the displacement between the grips. To calculate the strain, the distance between the grips was considered as initial gage length. Tests were carried out

Table 1. Controlled printing parameters

Parameter	0.2 mm Layer thickness		0.4 mm Layer thickness	
	Layers 1 to 3	Layers 4 to 35	Layers 1 and 2	Layers 3 to 18
Infill density (%)	100	100	100	100
Feed rate (mm/sec)	30	90	30	90
Extruder temperature (°C)	230	230	230	230
Bed temperature (°C)	70	110	70	110
Number of Shells	1	1	1	1

Table 2. Tensile test specimens in details.

0.2 mm Layer thickness		0.4 mm Layer thickness	
Number of layers	Nominal thickness	Number of layers	Nominal thickness
1	0.2	1	0.4
2	0.4	2	0.8
3	0.6	3	1.2
4	0.8	4	1.6
5	1.0	5	2
6	1.2	6	2.4
7	1.4	7	2.8
8	1.6	8	3.2
9	1.8	9	3.6
10	2	10	4
11	2.2	11	4.4
12	2.4	12	4.8
15	3	15	6
20	4	18	7.2
25	5		
30	6		
35	7		
Population per orientation	68	Population per orientation	56

according to ASTM D638 [21] at room temperature. The MTS pneumatic grips were displaced at the rate of 5 mm/min with data collected at 100 Hz. There are two important

outputs: load and displacement. To ensure that failure occurred in the gage section and that high grip pressure did not apply stress concentration on the specimens, grip pressure was manually controlled with the low at 173 KPa and the high at 275 KPa. To better understand the effects of layer thickness on failure modes of specimens, microscopic inspection was performed utilizing a Keyence VHX-600 digital microscope. Furthermore, air-gap to material ratio calculations on fracture surface areas of samples with 0.2 and 0.4 mm of layer thicknesses were done using a built-in function of the system's image processing software.

Finally, to demonstrate the approach in a more practical way, tensile tests were performed on an A-frame manufactured out of the same generic brand of ABS filament and under the same printing conditions (Table 1). Samples were printed in 0.2 and 0.4 mm layer thicknesses with different orientations using customized printing profiles of Makerware® software. Details on test samples for this case example are tabulated in Table 3. It should be noted that default orientation is a combination of 0°, 45°, and 90° orientations determined by Makerware® software. Figure 6 depicts the geometry of the proposed frame with its main dimensions. Testing was done utilizing the same MTS Insight 5 testing system with 5 mm/min displacement rate. In actual practice, functional parts endure two types of loading, static and dynamic. The A-frame is designed to serve as a functional static load-bearing structural component. A customized fixture was used in order to simulate a hypothetical working condition of the frame during testing. The test setup is shown in figure 7.

Table 3. Details of the A-frame samples for tensile test.

Layer thickness (mm)	
0.2	0.4
Orientation	Orientation
Default	Default
0°	0°
45°	45°
90°	90°

Sample size n = 3

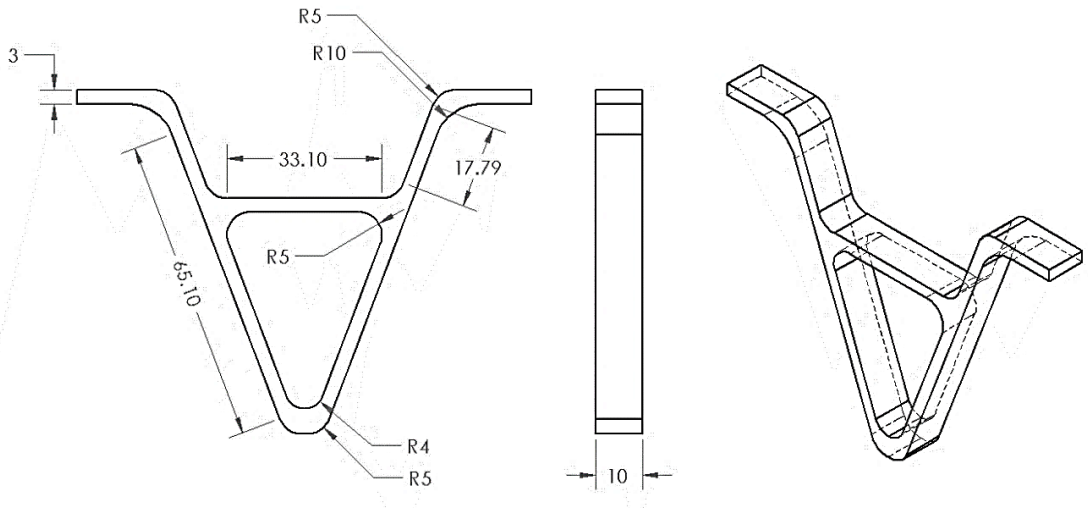

Fig. 6. A-frame geometry and its main dimensions in mm.

RESULTS AND DISCUSSION

TENSILE TEST RESULTS

An extensive experimental campaign was designed to study the effects of layer thickness on ultimate strength and elastic modulus of printed specimens at a range of layer thicknesses and raster orientations. Mean and standard deviation of test results are tabulated in Tables 4 and 5. To better understand the correlation between different thicknesses and orientations, graphical representations of the results are provided in

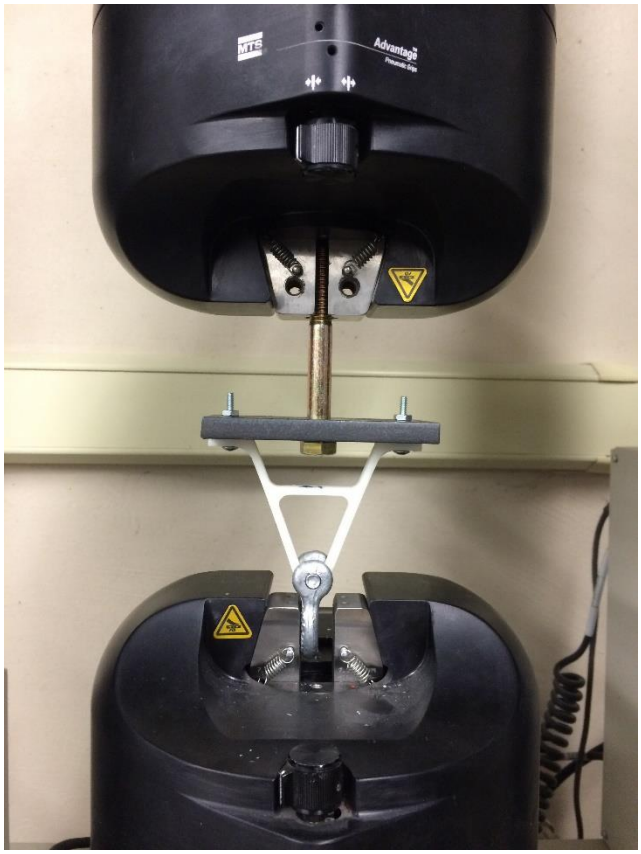

Fig. 7. Test setup for determining the strength of an A-frame as a functional load bearing part.

Figures 8 to 11. A first look at the results reveals that 0° raster orientation showed mostly the highest values for ultimate strength and elastic modulus for both 0.2 and 0.4 mm layer thicknesses, while 90° raster orientation resulted in the lowest values for ultimate strength and elastic modulus. For 45° raster orientation, these values mostly fell between those of 0° and 90° orientations. These results confirm previous work done in this area [4, 5, and 8].

This difference can be explained by considering inter-raster fusion bonds and tensile strength of each individual raster, known as trans-raster strength. The inter-raster fusion failure had the least influence on mechanical strength of specimens in 0° raster orientation, since each raster was pulled along its longitudinal axis, causing trans-raster

Table 4. Tensile test results for specimens with 0.2 mm layer thickness.

Number of Layers	0° Raster Orientation				45° Raster Orientation				90° Raster Orientation			
	Ultimate Strength (MPa)		Elastic Modulus (MPa)		Ultimate Strength (MPa)		Elastic Modulus (MPa)		Ultimate Strength (MPa)		Elastic Modulus (MPa)	
	Mean	σ	Mean	σ	Mean	σ	Mean	σ	Mean	σ	Mean	σ
1	32.2	6.4	1818.4	289.1	9.2	3.0	1219.5	177.0	3.9	1.0	550.3	151.5
2	30.3	1.4	1754.3	57.0	21.4	1.6	1561.5	97.6	12.1	1.1	1264.2	36.9
3	33.7	1.5	1812.9	47.7	23.8	4.2	1665.5	126.0	22.0	2.6	1519.5	20.0
4	32.9	1.7	1800.0	47.1	28.9	1.4	1755.2	88.2	26.4	0.4	1606.6	21.4
5	32.2	1.6	1750.6	57.1	30.0	1.3	1822.4	95.1	28.0	0.4	1682.1	36.3
6	35.4	1.6	1915.9	97.0	30.6	1.6	1801.1	106.4	28.2	0.7	2111.6	65.3
7	35.7	1.2	2107.3	79.2	30.8	0.9	1796.5	75.0	28.7	1.0	2125.3	92.2
8	35.5	1.7	2127.9	34.7	31.3	1.8	1979.9	64.7	30.3	0.3	2153.9	90.3
9	36.7	0.5	2055.7	105.3	32.2	1.4	2021.1	43.7	30.5	0.5	2196.1	50.0
10	37.2	0.2	2148.2	140.2	32.8	0.4	2092.0	73.0	31.3	0.1	2045.6	74.3
11	37.7	0.3	2093.9	99.0	34.3	0.6	2131.9	42.0	31.7	0.3	2103.0	44.6
12	37.5	0.6	2106.2	145.5	35.5	0.1	2224.8	72.7	31.3	0.1	2133.8	68.1
15	34.6	0.7	2123.9	50.6	34.1	0.2	2195.4	47.7	31.8	0.5	2193.7	45.8
20	38.7	0.8	2175.9	53.4	35.8	0.7	2193.1	92.2	31.6	0.4	2172.1	61.0
25	38.0	1.3	2160.0	83.1	36.1	0.3	2230.5	87.9	31.7	1.0	2140.9	61.5
30	38.7	0.6	2054.3	127.3	35.7	2.0	2128.0	67.8	32.5	0.4	2072.9	59.3
35	39.4	0.3	2221.3	90.6	35.8	0.1	2157.2	27.6	31.6	0.6	2076.1	104.2

Table 5. Tensile test results for specimens with 0.4 mm layer thickness.

Number of Layers	0° Raster Orientation				45° Raster Orientation				90° Raster Orientation			
	Ultimate Strength (MPa)		Elastic Modulus (MPa)		Ultimate Strength (MPa)		Elastic Modulus (MPa)		Ultimate Strength (MPa)		Elastic Modulus (MPa)	
	Mean	σ	Mean	σ	Mean	σ	Mean	σ	Mean	σ	Mean	σ
1	26.0	3.1	1604.1	91.9	14.5	2.3	1232.6	108.2	17.1	1.6	1397.4	123.5
2	29.0	1.6	1717.3	57.2	18.2	1.1	1325.0	48.1	24.1	0.6	1651.5	35.1
3	29.0	1.6	1741.2	37.0	23.1	0.4	1492.4	30.7	17.9	1.4	1317.6	47.0
4	29.2	2.6	1725.7	27.6	25.1	0.4	1545.1	10.9	27.8	0.5	1782.2	48.7
5	29.5	1.5	1757.5	27.8	27.6	0.4	1627.0	45.5	27.7	0.6	1766.1	14.4
6	29.8	1.2	1760.8	7.1	30.5	0.5	1775.4	50.0	28.0	0.2	1790.4	17.6
7	29.5	1.6	1772.6	12.7	29.5	0.2	1729.5	8.3	28.0	0.1	1764.7	23.8
8	30.3	0.7	1786.6	26.5	29.5	0.6	1708.8	33.8	26.9	0.4	1743.0	32.0
9	30.6	0.2	1803.6	5.6	29.4	0.7	1697.4	19.3	26.3	1.5	1767.9	49.6
10	32.0	1.4	1808.6	21.2	28.8	0.1	1721.3	25.4	27.5	0.2	1814.7	6.3
11	32.5	0.2	1749.5	27.1	28.3	1.4	1637.3	61.5	28.8	0.2	1785.4	43.4
12	32.4	0.9	1755.9	23.4	29.7	0.4	1750.4	49.3	28.1	0.3	1799.0	13.4
15	30.9	1.0	1678.7	57.9	29.1	1.3	1658.1	71.3	26.5	1.3	1787.2	30.3
18	33.0	0.6	1720.8	32.6	30.0	0.9	1652.7	30.0	28.4	0.1	1760.1	14.6

tensile failure. For specimens with 90° raster orientation, force was exerted perpendicular to raster longitudinal axis resulting in inter-raster fusion failure. In this case, layer adhesion along with the shell number in specimens with 90° raster orientation significantly affect the tensile strength, since the inter-raster fusion bonds between adjacent rasters withstood most of the applied load [2]. Figures 8 and 9 provide graphical comparison for data presented in Table 4 and 5. Comparison of 0.2 and 0.4 mm layer thicknesses showed that specimens with 0.4 mm layer thickness have less dependency on total thickness; whereas, specimens with 0.2 mm layer thickness displayed significant dependency on total thickness, particularly up to 2 mm total thickness. At thicknesses lower than 2 mm, failure at a raster or a layer will lead to failure of the entire specimen, since there is simply not enough remaining material to withstand the applied stresses. On the other hand, at thicknesses higher than 2 mm, the amalgamation of layers compensate for the failure of single rasters or layers and, as a result, the curve for both ultimate strength and elastic modulus plateaued throughout the test.

Figures 10 and 11 compare the strength of specimens with respect to their layer thickness. It is evident that specimens with 0.2 mm layer thickness displayed higher values for ultimate strength and elastic modulus than specimens with 0.4 mm. For a more in-depth study of this comparison, a numerical calculation of air-gaps was carried out using Keyence VHX-600 digital microscope images. Built-in image processing software provided area calculation options based on brightness and contrast differences. Two rectangular specimens were printed with the exact same settings in 0.2 and 0.4 mm layer thicknesses and 0° raster orientation (Fig. 12). In order to preserve the structural integrity of specimens and to ensure that the geometry of gaps was not affected when being cut, an

Instron Charpy impact tester was used to break specimens in half. Brittle fracture was ensured by cooling specimens to -29 °C. Air-gaps are generally categorized into three groups: 1) standard or zero, 2) positive, and 3) negative, as explained by Li et al. [23]. As depicted in Figure 12, rasters overlap each other when layers are deposited on top of one another, resulting in a negative air-gap. Based on the observation from these images, air-gaps appear periodically when the air-gap is negative. Results can be generalized for bigger cross sectional areas. Calculations were completed on 7.6 mm2 cross section area. As shown in Table 6, the air-gap to material ratio for 0.4 mm layer thickness specimen is 5.26%, while for 0.2 mm layer thickness it equals 0.3%. It can be concluded from the results that higher strength for specimens with 0.2 mm layer thickness is due to smaller air-gap to material ratio.

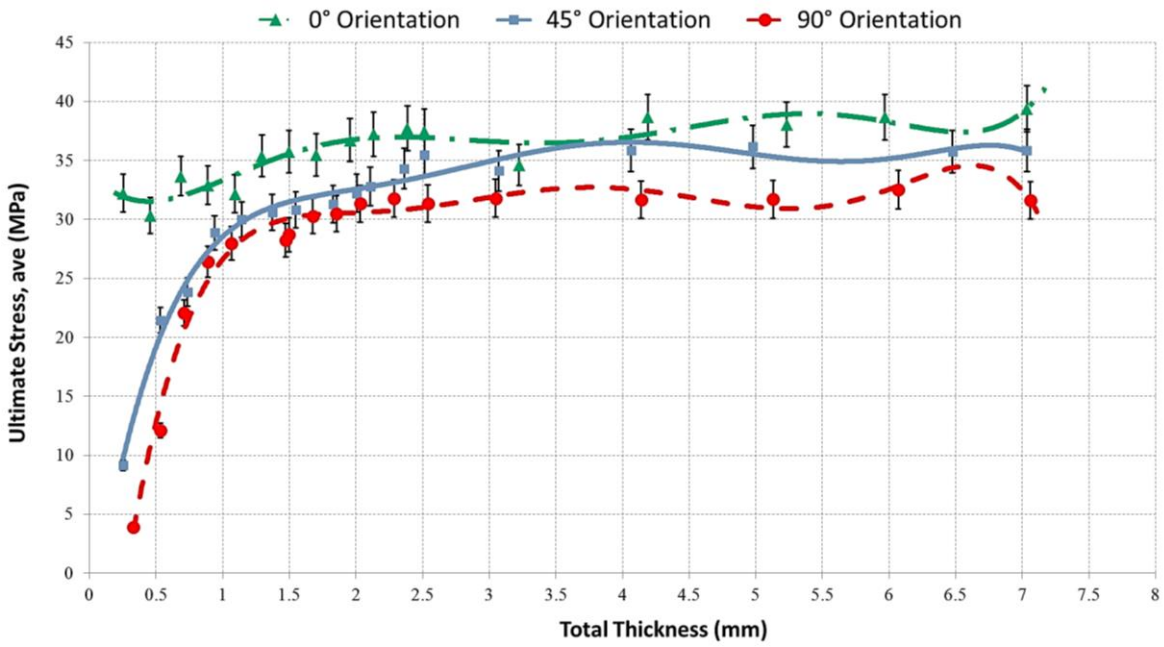

(a)

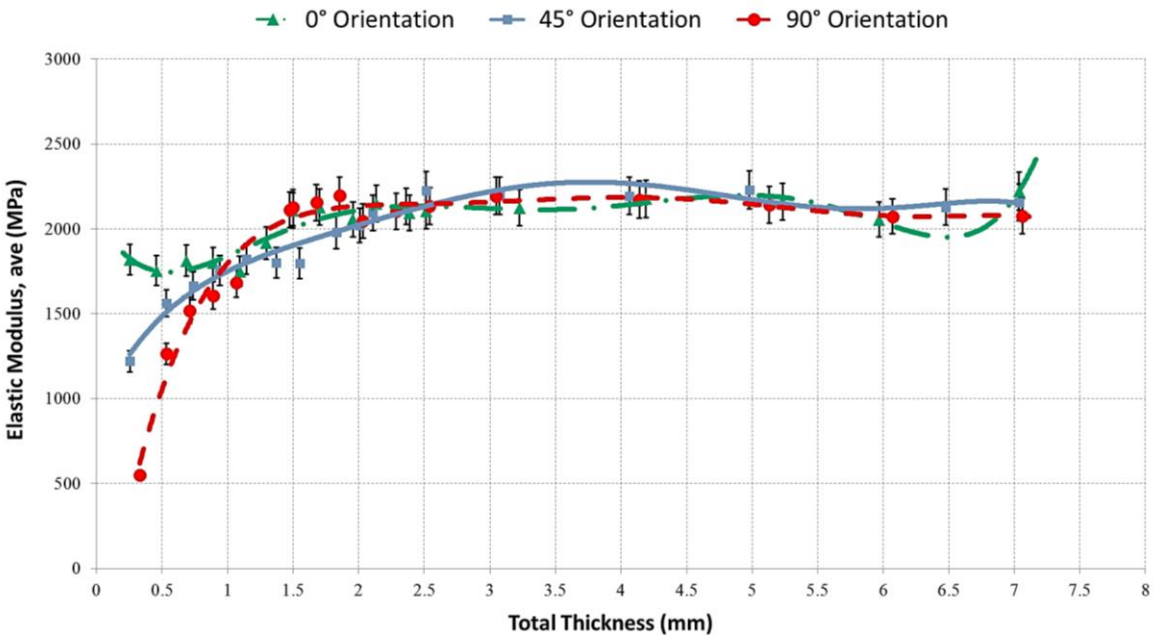

(b)

Fig. 8. Mechanical strength of specimens with 0.2 mm layer thickness with respect to the total thickness: (a). mean of ultimate strength vs. total thickness of samples. (b). mean of elastic modulus vs. total thickness of samples.

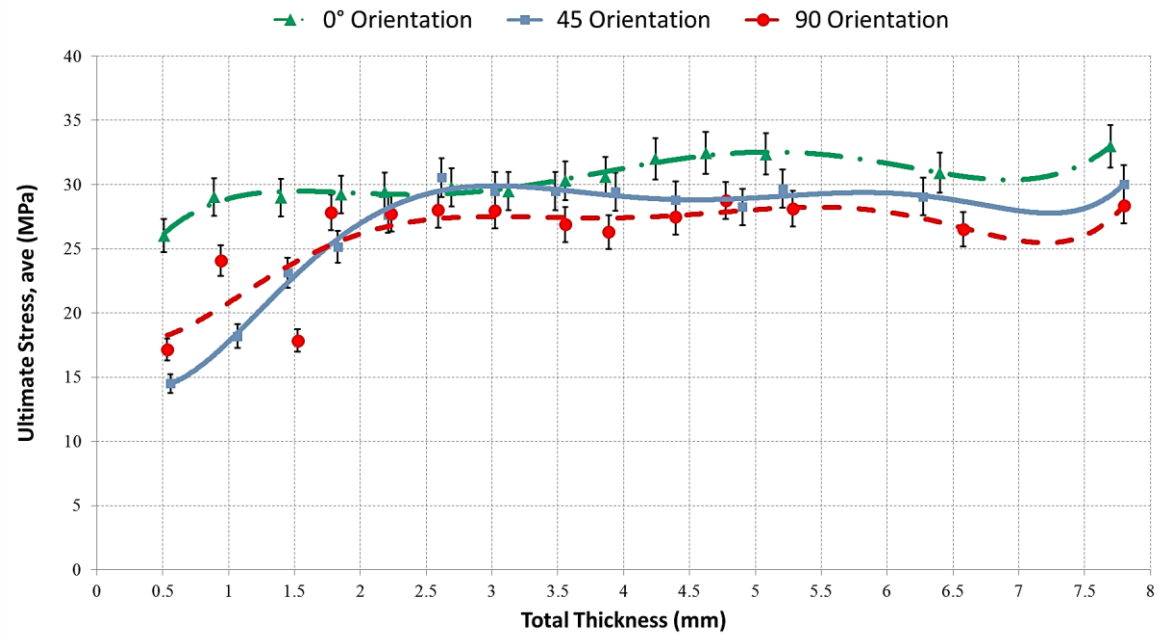

(a)

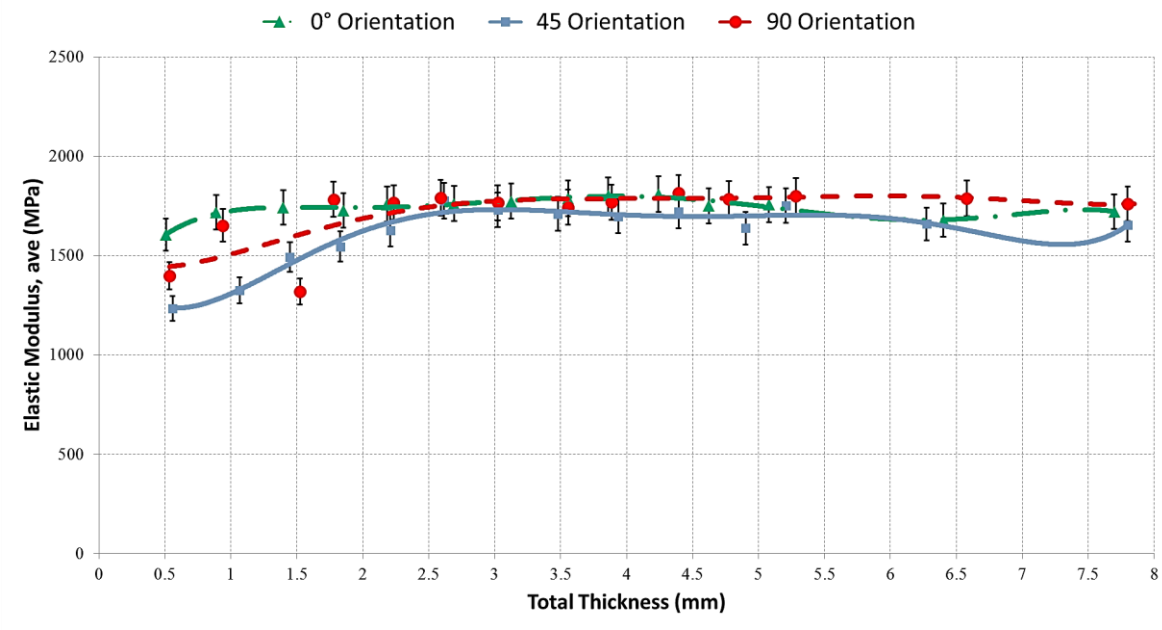

(b)

Fig. 9. Mechanical strength of specimens with 0.4 mm layer thickness with respect to the total thickness: (a). mean of ultimate strength vs. total thickness of samples. (b). mean of elastic modulus vs. total thickness of samples.

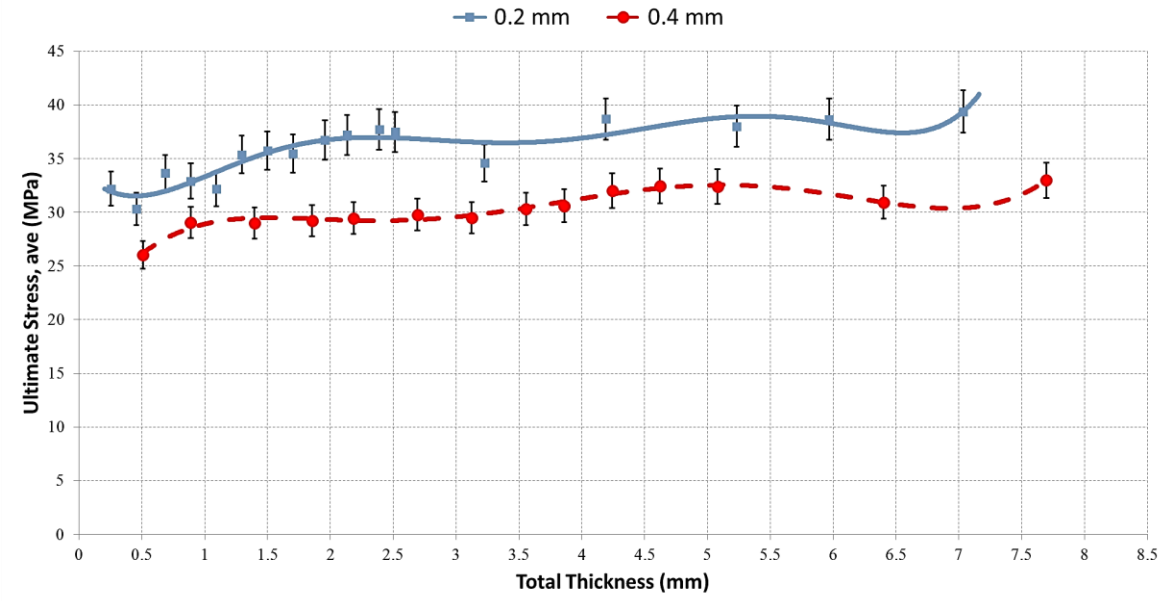

(a)

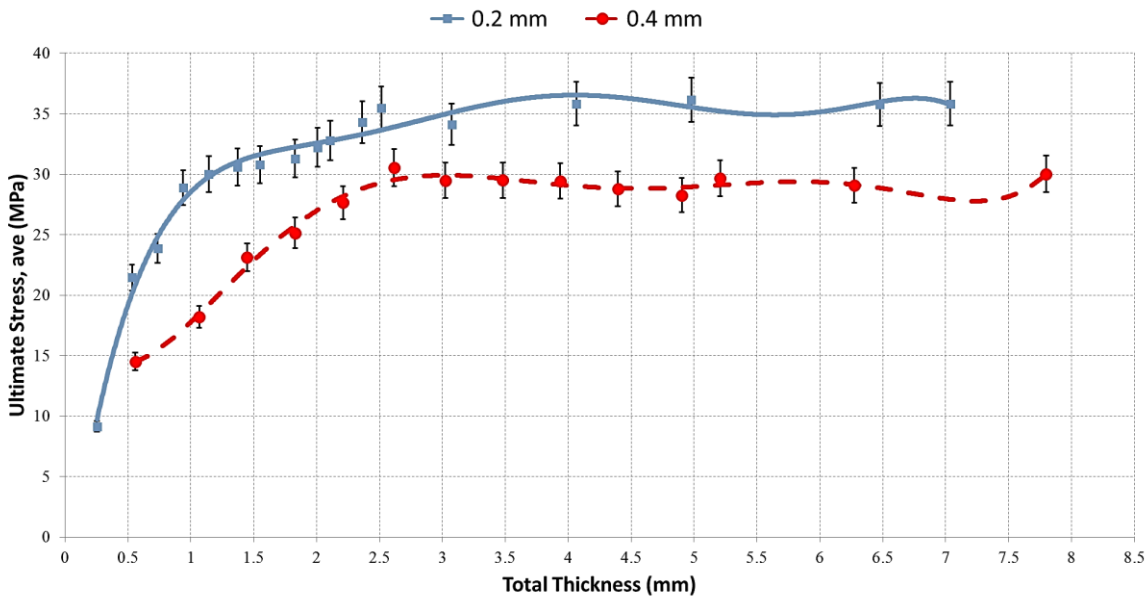

(b)

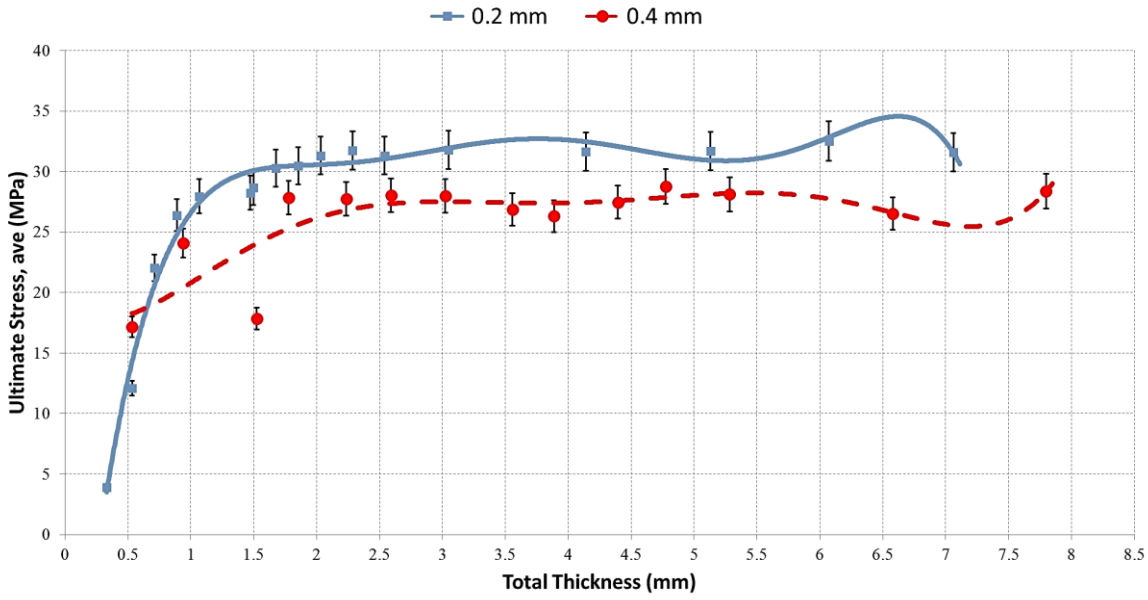

(c)

Fig. 10. Graphical comparison of ultimate strength for specimens printed at (a) 0° raster orientation (b) 45° raster orientation and (c) 90° raster orientation.

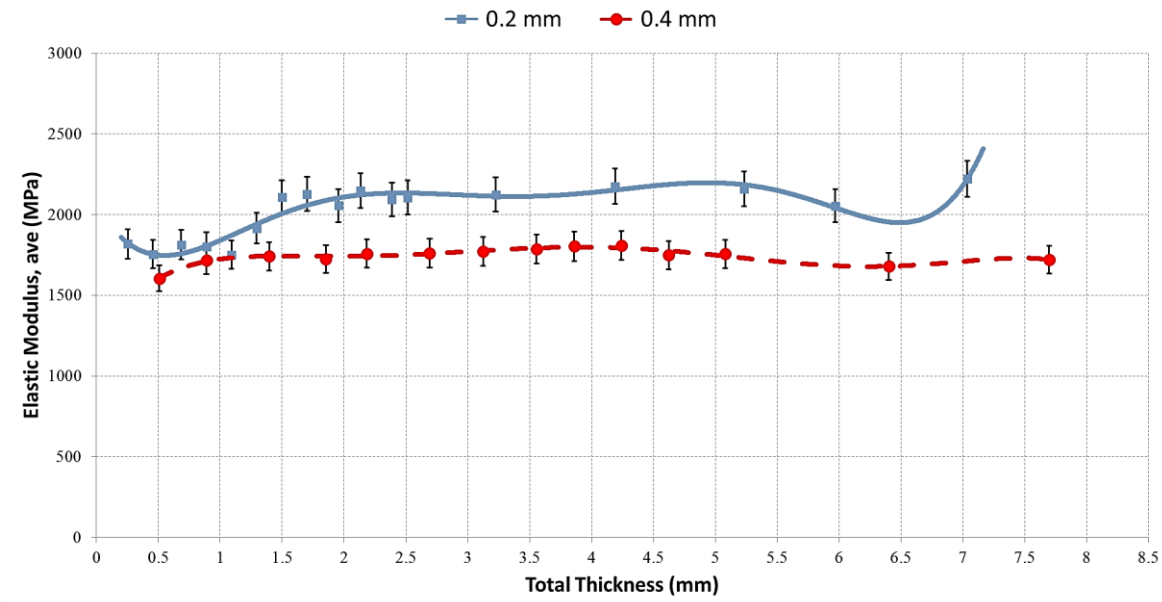
0.2 mm
0.4 mm
Elastic Modulus, ave (MPa)
Total Thickness (mm)
0
500
1000
1500
2000
2500
3000
0
0.5
1
1.5
2
2.5
3
3.5
4
4.5
5
5.5
6
6.5
7
7.5
8
8.5

(a)

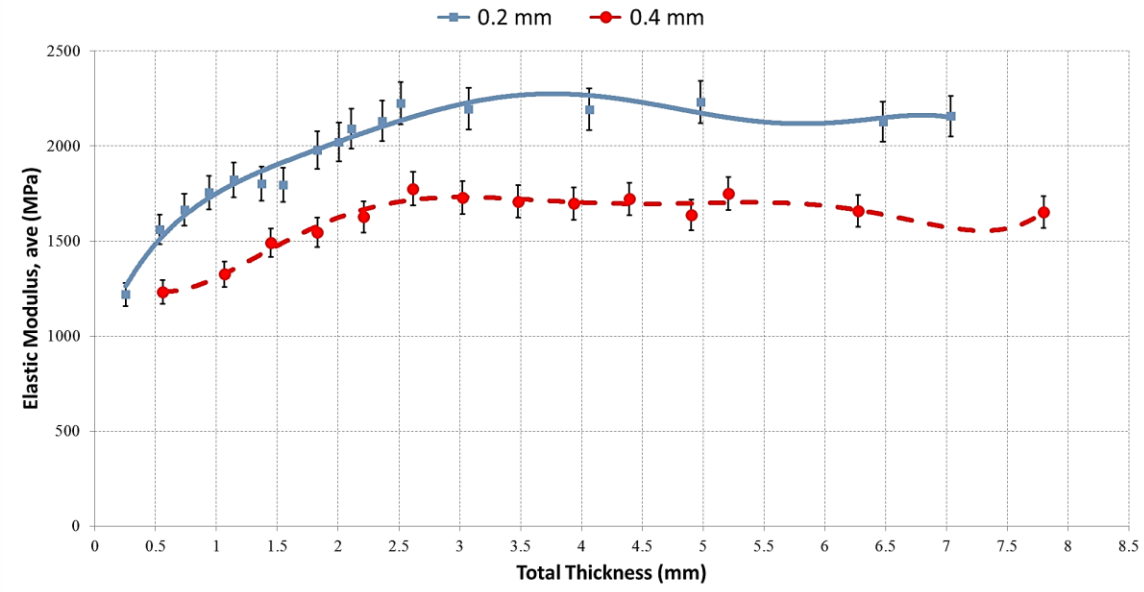
0.2 mm
0.4 mm
Elastic Modulus, ave (MPa)
Total Thickness (mm)
0
500
1000
1500
2000
2500
0
0.5
1
1.5
2
2.5
3
3.5
4
4.5
5
5.5
6
6.5
7
7.5
8
8.5

(b)

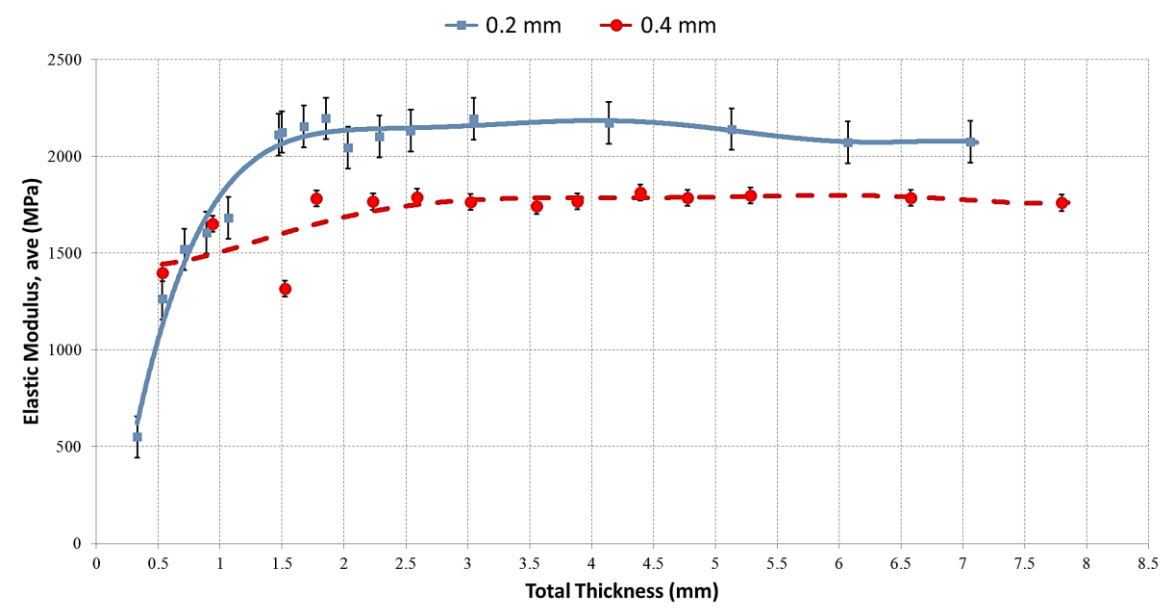

(c)

Fig. 11. Graphical comparison of elastic modulus for specimens printed at (a) 0° raster orientation (b) 45° raster orientation and (c) 90° raster orientation.

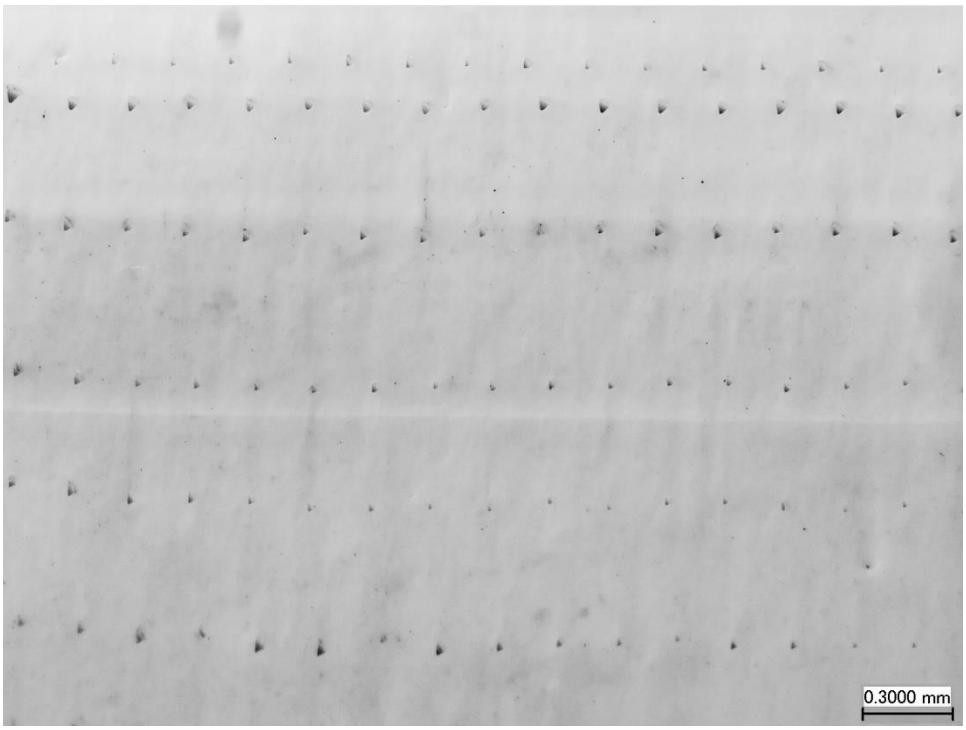

(a)

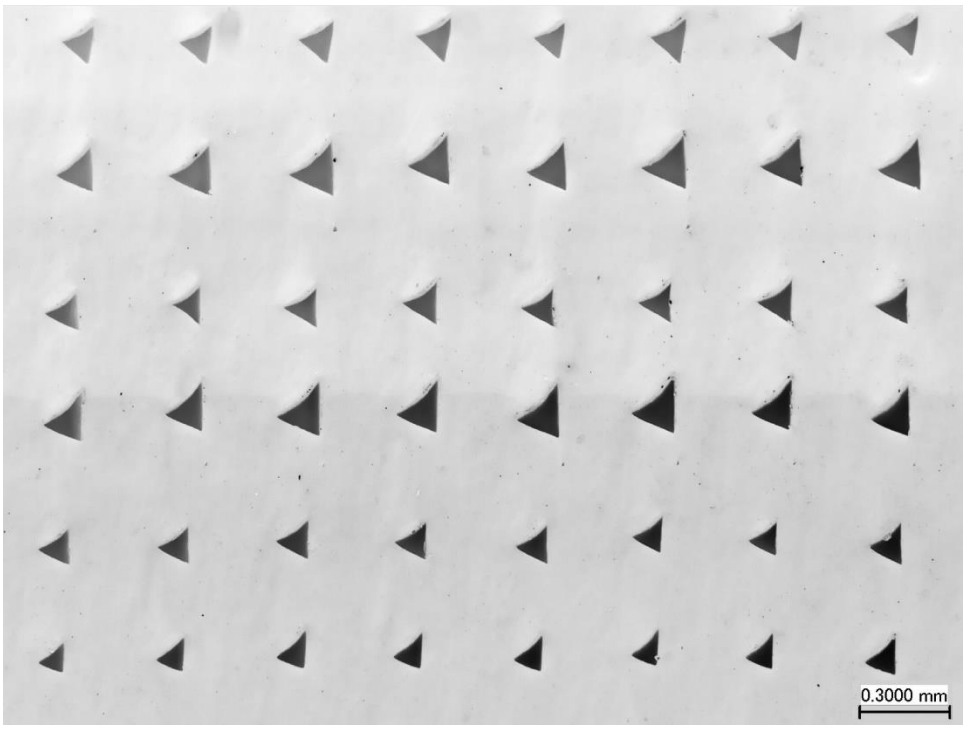

(b)

Fig. 12. Mesostructures of air-gaps for specimens with (a) 0.2 mm and (b) 0.4 mm layer thickness.

Table 6. Air-gap to material ratio calculation for specimens printed at 0° raster orientation.

Calculated property	0.2 mm layer thickness	0.4 mm layer thickness
Inspected area (mm^2)	7.6038	7.6038
Total air-gap area (mm^2)	0.0232	0.4
Number of air-gaps	218	182
Air-gap to material ratio (%)	0.3	5.26

STATISTICAL ANALYSIS

Full factorial regression models were built and used for ANOVA analyses to investigate the effects of layer thickness and raster orientation on mechanical properties

of tensile test specimens, including elastic modulus and ultimate strength. Table 7 shows the factors in the models and their corresponding levels. Furthermore, the results from ANOVA analyses are provided in Table 8. Since the significance level (α) used in the analyses is set to 0.05, any factor or combination of factors having a P value of 0.05 or less is considered to have a significant effect on the responses (mechanical properties), with the highest F value, having the most significance. Consequently, in the ANOVA analysis for elastic modulus, the only significant source was found to be the layer thickness. In the case of ultimate strength, however, layer thickness and orientation and also their combination were found to be significant, with the layer thickness having the most significant effect. The effect from the combination of factors was concluded to be marginal as its F value is relatively small when compared to those of the main effects of factors; hence, its significance originates from the significance of each individual factor.

Table 7. List of factors and their levels.

Factor	Levels	Values
Layer thickness (LT)	2	0.2 mm, 0.4 mm
Orientation (O)	3	0°, 45°, 90°

Table 8. ANOVA analyses results

Source	DOF	Elastic Modulus (MPa)				Ultimate Strength (MPa)			
		SS	MS	F	P (> F)	SS	MS	F	P (> F)
LT (mm)	1	1232036.90	1232036.90	335.8	< 0.0001	159.738	159.738	573.55	< 0.0001
O (Degree)	2	21649.359	10824.679	2.95	0.0779	150.421	75.211	270.05	< 0.0001
LT x O	2	21906.664	10953.332	2.99	0.0759	10.323	5.162	18.53	< 0.0001
Error	18	66027.912	3668.217	-	-	5.013	0.279	-	-

In addition to ANOVA analyses, all pairs Tukey-Kramer analyses were performed to determine how a change in significant factors would affect the mechanical properties and which specimens have the highest mechanical properties. Factors included in the models used for Tukey-Kramer analyses were chosen according to the results of the ANOVA table. Hence, for elastic modulus, results were compared based on the effect of the change in layer thickness only, while for ultimate strength, the effects of both layer thickness and orientation were considered. As can be seen in Figure 13, the results of Tukey-Kramer tests from samples of 0.2 mm layer thickness have a significantly higher elastic modulus than those of 0.4 mm layer thickness. Ultimate strength has the highest value and is significantly different for samples with 0.2 mm layer thickness and 0° raster orientation. Samples with 0.2 mm layer thickness have significantly higher ultimate strengths compared to those with 0.4 mm layer thickness, except for 0.2 mm and 90° orientation which have slightly lower ultimate strengths than 0.4 mm and 0° raster orientation. For each layer thickness, ultimate strength is the highest for 0° raster orientation and keeps decreasing constantly when it is changed to 45° and then 90°. Samples with 0.4 mm layer thickness and 90° raster orientation have the lowest ultimate strengths, which are significantly lower than those of all other samples.

MICROSCOPIC INSPECTION

The fracture surface of specimens with 15 layers (at 0.2 mm layer thickness) and 9 layers (at 0.4 mm layer thickness) used as representatives of the entire population, are provided in Figures 14 and 15, respectively. Comparison of fracture morphologies showed that failure modes are independent of layer thickness and change with respect to raster orientation. A comparison of Fig.14 (a) and Fig. 15(a) reveals the effect of larger

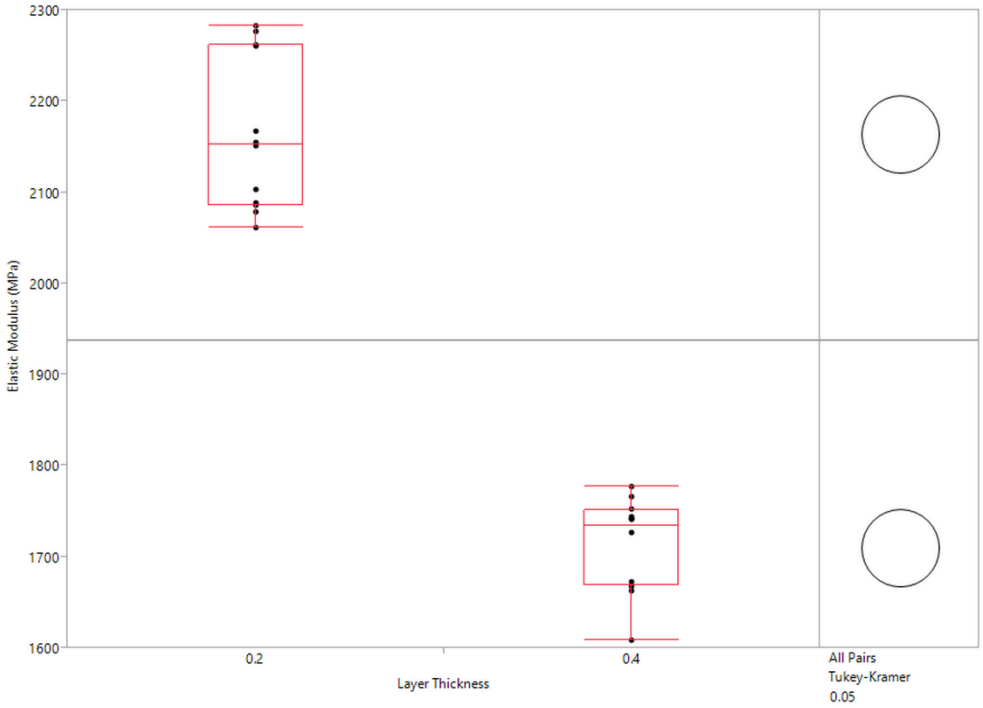

(a)

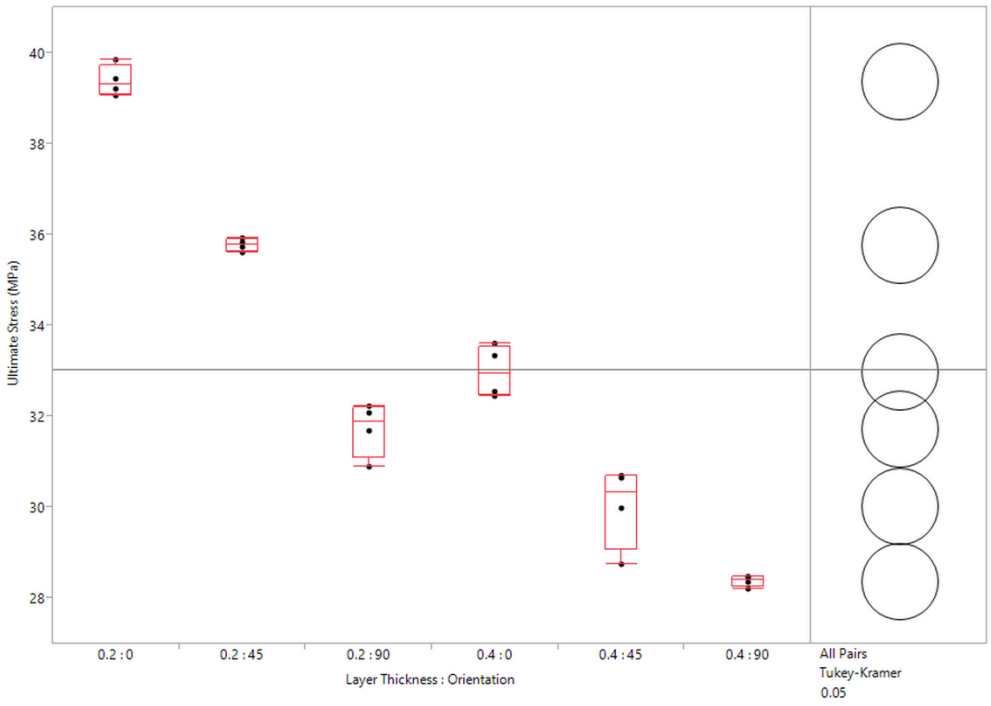

(b)

Fig. 13. Tukey-Kramer results (a) Elastic Modulus vs. Layer Thickness (b) Ultimate Strength vs. Layer Thickness and Orientation.

air gaps on the fracture morphology of the specimens. It can be seen that larger air-gaps in the specimen with 0.4 mm layer thickness caused inter-raster fusion bonds to fail resulting in a more discretized surface area. Failure at specimens with 0° raster orientation is mainly associated with trans-raster failure which agrees with their resulting higher tensile strength. On the other hand, specimens with 90° raster orientation experienced a more brittle fracture since failure occurs mainly in inter-raster fusion bonds as shown in Fig. 14(c) and Fig. 15(c). This conclusion also agrees with results obtained from tensile tests. Overall, there are two main failure modes for tested specimens: 1) inter-raster fusion bond failure, which is the main contributor to failure of samples printed in 45° and 90° raster orientations, regardless of their layer thickness; and 2) trans-raster failure, which is the main contributor to failure of specimens printed in 0° raster orientation, regardless of their layer thickness [24].

THE A-FRAME TEST RESULTS

An arbitrary “A” shaped structural frame was designed and manufactured using the same printing settings mentioned in Table 1. Table 9 shows the mean and standard deviation for the maximum force at failure for each orientation and layer thickness. Due to the geometry of the part, instead of calculating stress, the maximum load at failure was considered for strength comparison. As expected from the tensile test results, samples with 0.2 mm layer thickness demonstrate higher mechanical strength compared to samples with 0.4 mm layer thickness. Effects of raster orientation are also as expected, with default orientation resulting in the highest value for force at failure, following by 0°

orientation (Fig. 16). However, unlike the tensile test samples, the combination of layer thickness and raster orientation rather than layer thickness alone, have a significant effect on the final strength of the material due to complex geometry of the frame.

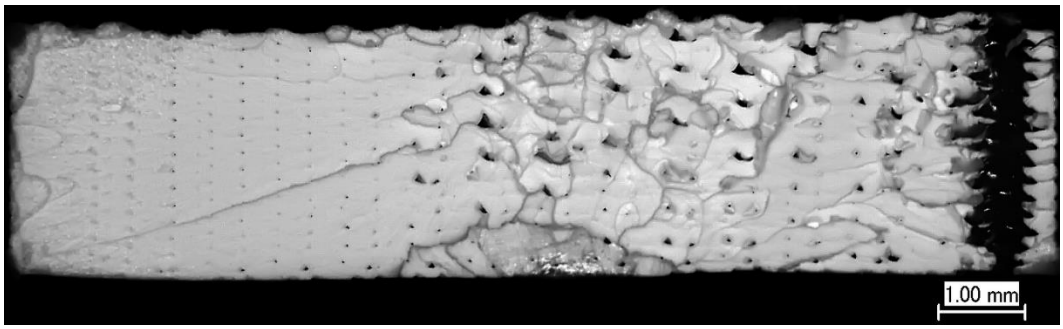

(a)

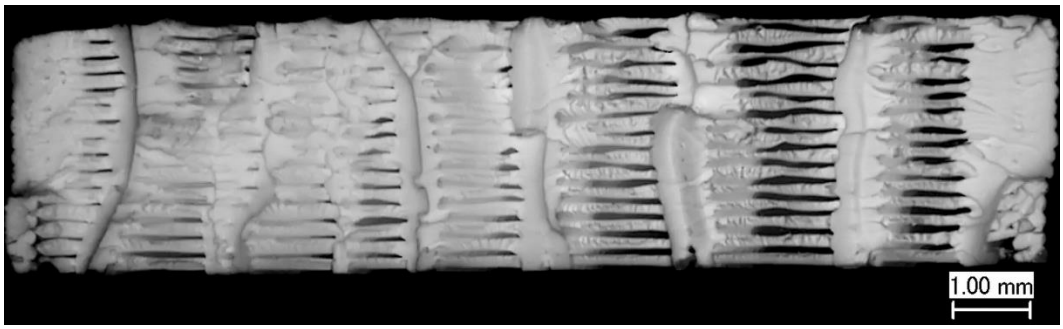

(b)

(c)

Fig 14. Microscopic inspection of failure area of 0.2 mm layer thickness specimens at different orientations at 20x: (a) 0° raster orientation, (b) 45° raster orientation, (c) 90° raster orientation

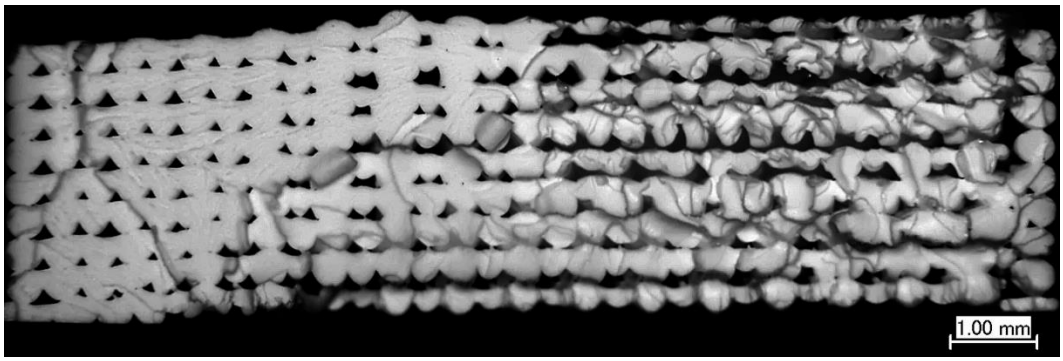

(a)

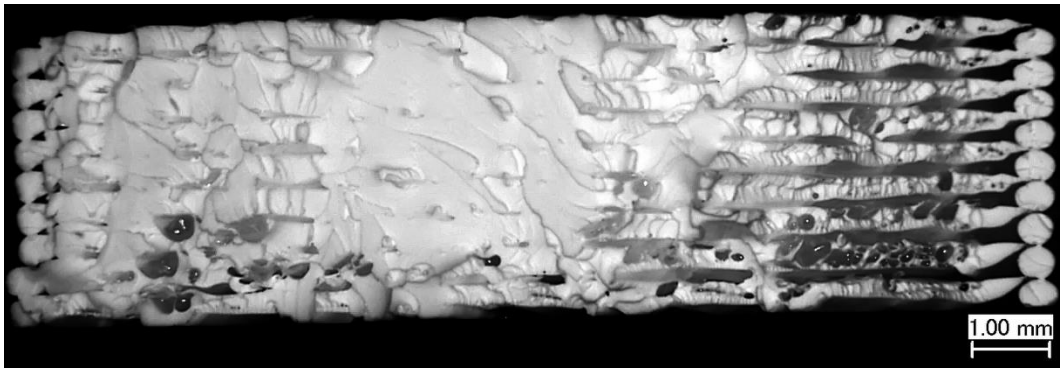

(b)

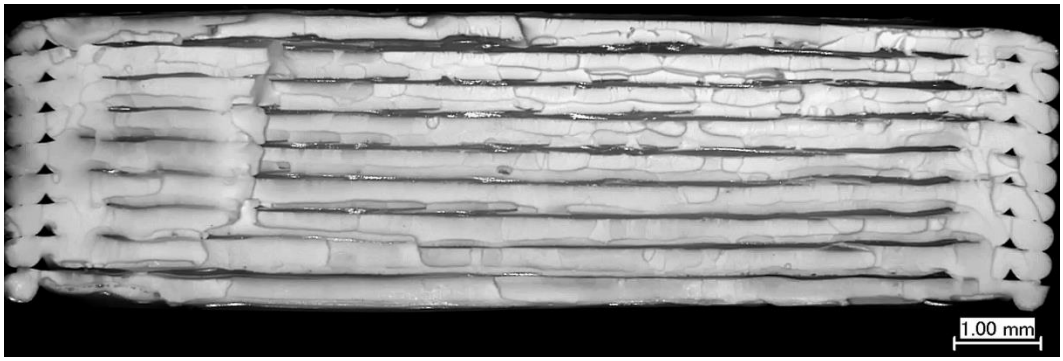

(c)

Fig 15. Microscopic inspection of failure area of 0.4 mm layer thickness specimens at different orientations at 20x: (a) 0° raster orientation, (b) 45° raster orientation, (c) 90° raster orientation

Table 9. Tensile test results for the a-frame.

Raster orientation	Maximum force (N)			
	0.2 mm layer thickness		0.4 mm layer thickness	
	Mean	σ	Mean	σ
Default	1223.6	41.1	1130.9	36.2
0°	1120.9	33.3	1011.3	49.1
45°	1107.8	17.9	828.9	72.8
90°	1104.4	92.8	995.7	83.1

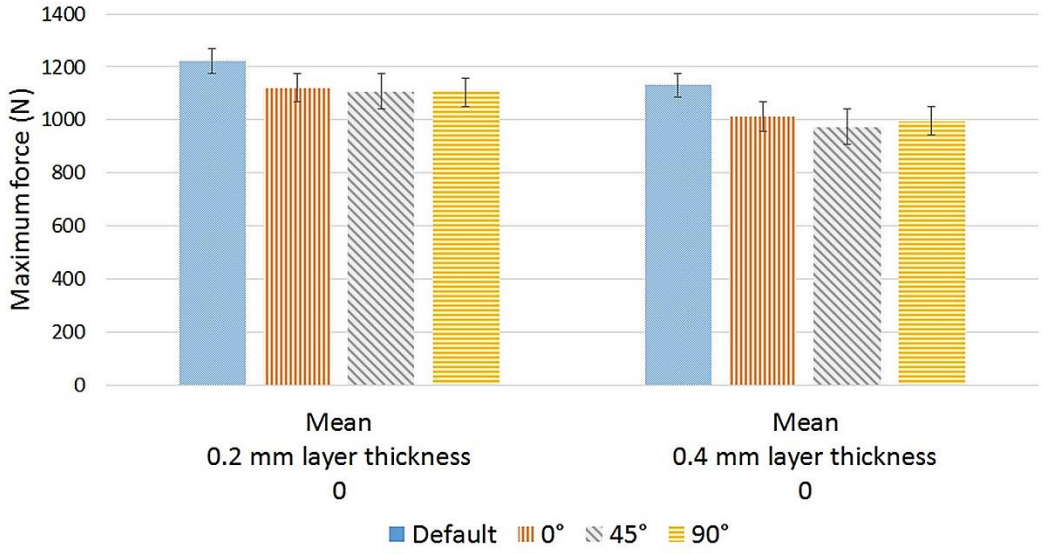

Fig. 16. Comparison of the A-frame tensile test results.

CONCLUSION

The effects of layer thickness and raster orientation on mechanical properties of 3D printed specimens were studied by running an extensive experimental campaign in order to address the controversy in the literature regarding the effects of layer thickness. Tensile test results along with statistical analyses of the data clearly suggest that

specimens with 0.2 mm layer thickness are stronger than specimens with 0.4 mm layer thickness and that layer thickness and raster orientation both have a significant effect on the mechanical properties of material. This conclusion was also confirmed by testing an A-frame as a practical 3D printed part. The microscopic inspection of fracture area revealed that smaller air-gap to material ratio can be the main factor contributing to higher strength in these specimens.

As the FDM advances into a more practical and industrial method of manufacturing, in-depth understanding of less known printing parameters, such as layer thickness on the strength of the end user part, becomes paramount. The purpose of this study was to provide solid ground for designers and manufacturers on which they can make better engineering decisions by having all required information at hand.

REFERENCES

[1] "Standard Terminology for Additive Manufacturing Technologies, (Withdrawn 2015)", ASTM F2792-12a, ASTM International, West Conshohocken, PA, 2012.

[2] T. Letcher, B. Rankouhi and S. Javadpour, Experimental study of mechanical properties of additively manufactured ABS plastic as a function of layer parameters, ASME 2015 Int. Mech. Eng. Cong. and Exp., 2015, p. V02AT02A018-V02AT02A018.

[3] "Wohler's Report, 3D Printing and Additive Manufacturing State of the Industry, Annual Worldwide Progress Report", 2014, Wohler's Associates, 2015, p. 20.

[4] B. M. Tymrak, M. Kreiger, and J. M. Pearce, Mechanical properties of components fabricated with open-source 3-D printers under realistic environmental conditions, Mat. Des., Vol. 58, 2014, p. 242-246.

[5] Angel R. Torrado, and David A. Roberson. Failure analysis and anisotropy evaluation of 3D-printed tensile test specimens of different geometries and print raster patterns. J Fail. Anal. And Preven., Vol. 16 (1), 2016, p 154-164.

[6] D. Croccolo, M. De Agostinis, and G. Olmi, Experimental characterization and analytical modelling of the mechanical behaviour of fused deposition processed parts made of ABS-M30, Comp. Mat. Sci., Vol. 79, 2013, p. 506-518.

[7] A. Bellini, S. Güçeri, Mechanical characterization of parts fabricated using fused deposition modeling, Rap. Proto. J., Vol. 9(4), 2003, p. 252-264.

[8] S. Ahn, M. Montero, D. Odell, S. Roundy and P. K. Wright, Anisotropic material properties of fused deposition modeling ABS, Rap. Proto. J., Vol. 8(4), 2002, p. 248-257.

[9] J. F. Rodríguez, J. P. Thomas, J. E. Renaud, Design of fused-deposition ABS components for stiffness and strength. J. Mech. Des., Vol. 125(3), 2003, p. 545-551.

[10] E. Ulu, E. Korkmaz, K. Yay, O. B. Ozdoganlar, and L. B. Kara, Enhancing the structural performance of additively manufactured objects through build orientation optimization, J. Mech. Des., Vol. 137(11), 2015, p. 111410-111410-9.

[11] B. H. Lee, J. Abdullah, and Z. A. Khan. Optimization of rapid prototyping parameters for production of flexible ABS object, J. Mat. Proc. Technol., Vol. 169(1), 2005, p. 54-61.

[12] A. K. Sood, R. K. Ohdar, and S. S. Mahapatra, Parametric appraisal of mechanical property of fused deposition modelling processed parts. Mat. Des., Vol. 31(1), 2010, p. 287-295.

[13] R. Anitha, S. Arunachalam, and P. Radhakrishnan, Critical parameters influencing the quality of prototypes in fused deposition modelling, J. of Mat. Proc. Technol., Vol. 118(1-3), 2001, p. 385-388.

[14] M. Vaezi, and C. K. Chua, Effects of layer thickness and binder saturation level parameters on 3D printing process, Int. J. Adv. Manuf. Technol., Vol. 53(1), 2011, p. 275-284.

[15] R. R. Ma, L. U. Odhner, and A. M. Dollar, A modular, open-source 3d printed underactuated hand, Robot. Auto. (ICRA), IEEE Int. Conf., 2013, p. 2737-2743.

[16] J. Won, K. DeLaurentis, and C. Mavroidis, Rapid prototyping of robotic systems, IEEE Int. Conf. Rob. Auto., 2000, Vol. 4, p. 3077-3082.

[17] K. J. De Laurentis, F. F. Kong, and C. Mavroidis, Procedure for rapid fabrication of non-assembly mechanisms with embedded components, ASME Int. Des. Eng. Tech. Conf. Comp. Info. Eng. Conf., 2002, p.1239-1245.

[18] J. T. Belter, A. M. Dollar, Strengthening of 3D printed fused deposition manufactured parts using the fill compositing technique. PLoS ONE, Vol. 10(4), 2015, e0122915.

[19] Y. Jin, J. Plott, R. Chen, J. Wensman, and A. Shih, Additive manufacturing of custom orthoses and prostheses–A review, Procedia CIRP, Vol. 36, 2015, p. 199-204.

[20] S. Telfer, J. Pallari, J. Munguia, K. Dalgarno, M. McGeough, and J. Woodburn, Embracing additive manufacture: implications for foot and ankle orthosis design, BMC musc. Dis., Vol. 13(1), 2012, p. 1-9.

[21] "Standard test method for tensile properties of plastics", ASTM D638-14, ASTM International, West Conshohocken, PA, 2014.

[22] "Standard test method for tensile properties of polymer matrix composite materials", ASTM D3039/D3039M – 14, ASTM International, West Conshohocken, PA, 2014.

[23] L. Li, Q. Sun, C. Bellehumeur, & P. Gu, Composite modeling and analysis for fabrication of FDM prototypes with locally controlled properties. J. Manuf. Proc., Vol. 4(2), 2002, p. 129-141.

[24] A. R. Torrado Perez, D. A. Roberson, and R. B. Wicker, Fracture surface analysis of 3D-printed tensile specimens of novel ABS-based materials, J. Fail. Anal. Preven., Vol. 14(3), 2014, p. 343-353.

CHAPTER 2

AN EXPERIMENTAL INVESTIGATION OF THE EFFECTS OF GAMMA IRRADIATION ON ABS AND CARBON FIBER REINFORCED ABS SAMPLES MADE BY FDM

INTRODUCTION

After almost three decades of latency, space exploration is once again flourishing. With a mission to Mars on NASA's horizon and major achievements of private sector in developing new means of space travel, such as re-usable rockets and novel propulsion systems, the future of space exploration looks more promising than before. In the midst of these developments, additive manufacturing experienced an upsurge with the advent of desktop 3D printers [1]. These printers are capable of creating complex geometries using a wide range of thermoplastics. They are fast compared to conventional manufacturing methods, use considerably small amount of material, and produce almost no waste during the manufacturing process, in addition they are relatively low cost and small in size. These attributes make desktop 3D printers an excellent candidate for in-space manufacturing, a term that encompasses the most recent advancements in the fields of manufacturing and aerospace. Although the idea of manufacturing parts in space is exhilarating, many obstacles must be overcome before the technology comes to full fruition. One of these obstacles is the effects of space radiation on additively manufactured parts and feedstock in low-earth orbit and beyond. Functional 3D printed parts can be used on-board a space craft, in deep space as a functional part of a satellite and on the surface of Moon or Mars where radiation effects are a major concern. The effects of space radiation on the human body has been the main focus of scientists in the discipline of radiation protection [2-6]. Although some studies have looked at the effects of space environment on polymers and polymer composites [7 and 8], the effects of these radiations on material properties and mechanical performance of a functional part which

is additively manufactured have yet to be thoroughly investigated since the were no need for such experiments until recently.

Rochus et al. [9] investigated the applications of Additive Manufacturing (AM) for space instrumentation. They concluded that several types of AM techniques, including FDM, can be made applicable to the space sector. While cleanliness and vacuum resistance were considered as requirements in their study, radiation resistance was left out. In 2014, Beyer [10] predicted that AM will greatly impact the future of aerospace industry. Guo and Leu [11] called the AM technology highly suitable for aerospace applications. Moreover, Made In Space introduced and implemented the first microgravity FDM 3D printer in 2014 [12]. With its second generation machine operating on board the International Space Station (ISS), new opportunities are available to us to take the first necessary steps toward in-space manufacturing and eventually earth independency for deep space explorations. Tethers Unlimited Inc. has already taken the first step with an attempt to utilize FDM technology for in-space manufacturing [13]. Their proposed architecture seeks to adapt the AM techniques and robotic assembly technologies to fabricate and integrate large space systems in orbit using polymer-based composites. Understanding the hazards of space environment and their impact on properties of parts fabricated using AM will soon become necessities. This work is a prelude to a more in-depth study of space radiation effects on various parts manufactured using FDM technique.

SPACE RADIATION

In order to study the effects of radiation on the mechanical properties of materials, particularly 3D printed parts, the nature, types and dosage of radiations which exist off

the earth must be addressed. Figure 1 shows the three primary sources of ionizing radiation in Low Earth Orbit (LEO): (1) Galactic Cosmic Rays (GCRs) which permeate throughout space from unknown sources beyond our solar system. They consist of 85-90% protons, 10-13% Helium ions and 1% electrons, (2) trapped radiation which are energetic electrons and protons trapped in the Earth's geomagnetic field, and (3) solar energetic particles (SEPs) which are charged particles composed of mostly protons, electrons, helium ions and highly energetic particles in the heavy ion component (HZE particles). SEPs are normally caused by solar flares and coronal mass ejections (CMEs) [14 and 15]. In addition to these three principal sources, secondary particles are of importance. These particles are the product of nuclear reaction between the primary particles and the constituent nuclei of the spacecraft exposed to any type of ionizing radiation [14]. Unlike GCRs and SEPs, secondary particles and trapped radiation do not exist in interplanetary space.

Radiation exposure poses a much higher threat on the surface of Mars than on Earth, for two reasons: Mars lacks a magnetic field, and its atmosphere is much thinner (<1%) than that of Earth leaving Mars' surface defenseless against any type of radiation. GCRs and SEPs are also the main sources of radiation on the surface of Mars. If they penetrate into the Martian regolith, they can produce secondary particles including gamma rays and neutrons [15].

Parts, such as tools, basic surgical instruments, containers and spares are being tested to be used on board the ISS. FDM can also be used in open space as a functional part installed on a satellite or on the surface of Mars as a functional part of a rover. Since 3D printed parts can be used for a variety of applications in space and on board the ISS, it

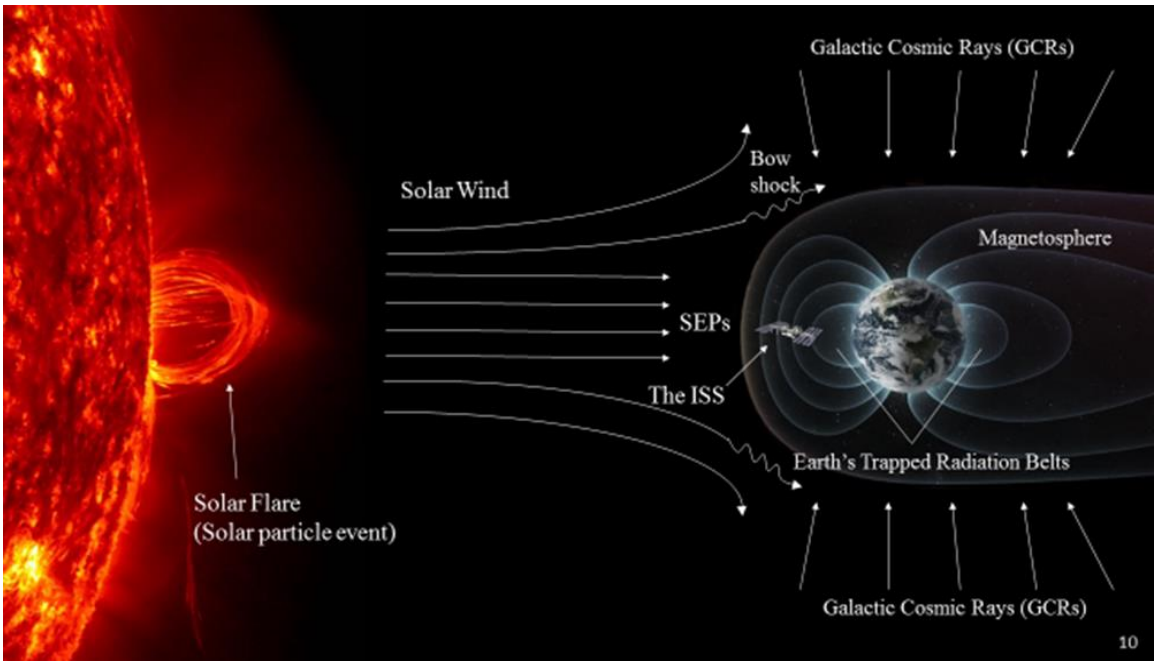

Fig. 1. Three primary sources of ionizing radiation. All three are affected by the Earth's magnetic field. The ISS is still exposed to GCRs and SEPs even though it is protected by the Earth's magnetic field (not to scale) [14].

is paramount to know the radiation dose rate in these environments (dose is energy per unit mass expressed in units of Gray where 1 Gy = 1 J/kg = 100 rad). The radiation environment in LEO, deep space, on board the ISS and on the surface of Mars is very dynamic, making accurate measurements difficult. Moreover, means of measuring the radiation dosage have changed throughout the years and, as a result, a wide range of data have been produced since the early Russian and US dose measurements in 1960 [14]. In this study, to provide a high margin of safety, the worst case scenarios were chosen for comparison, where the highest radiation dose was detected. Table 1 shows the maximum collected dose rate abroad the ISS, in LEO and during significant flight missions. Table 2 shows the maximum dose rate on the surface of Mars as well as in transit to Mars collected by Mars Science Laboratory's Curiosity rover.

Table 1. Mean dose rate measurements on Russian and US missions, on board the ISS and in LEO using different dosimetry methods [14 and 16].

Mission/Space craft	Year	Mean dose rate (μGy/day)
Voskhod-2	1965	650
Apollo 14	1971	1270
Mir-15	1994	508
EuroMir 95	1995	483
NASA-4/Mir-23	1997	375
ISS-Russian service module Zvezda	-	299
Outside the ISS-MATROSHKA	-	510

Table 2. Mars radiation environment summary during 2012-2013 solar maximum for GCR and SEP with mean daily average of radiation throughout 2012-2013 [15].

	GCR dose rate (mGy/day)	SEP dose (mGy/event)	Mean dose rate (mGy/day)
MSL Cruise	0.464	1.2 to 19.5	0.48
Mars Surface	0.21	0.025	0.21

EXPERIMENTAL SETUP

The goal of this study was to investigate the mechanical properties degradation of 3D printed ABS and carbon fiber reinforced ABS exposed to gamma irradiation to simulate the space radiation environment and its effects for future in-space manufacturing. To do so, tensile and flexural tests were designed in two different scenarios. First, tests were performed on manufactured samples after being irradiated by gamma rays. In this scenario authors tried to investigate whether samples that were made by FDM in a shielded environment are able to maintain their structural performance after absorbing radiation in space. Second, tests were performed on samples that were manufactured from irradiated filament. In this case, authors tried to address the benefits

of AM from the perspective of logistics. The ability to produce specific, useful components from undifferentiated feedstock will be a game changer for future space missions. That is if the feedstock maintain its printability after absorbing radiation and, if the manufactured parts show the same mechanical performance as their counterparts made from non-irradiated filament.

Two different feedstock materials were considered as candidates for this study: Acrylonitrile Butadiene Styrene (ABS) and carbon fiber reinforced ABS (CF-ABS). ABS was chosen because it was the first thermoplastic polymer that was used (and is still being used) on board the ISS to build functional parts (Fig. 2). CF-ABS was chosen because hybrid materials such as polymer matrix composites have been proposed for variety of space applications such as large, high performance truss structures [13].

Fig. 2. International Space Station Expedition 42 Commander Barry "Butch" Wilmore shows off a ratchet wrench made with the first FDM 3D printer on the station [17].

To prepare the ABS samples, ASTM D638 [18] and ASTM D790 [19] guidelines were used for tensile and flexural test specimens, respectively. ASTM D3039 [20] and ASTM D790 [19] were followed for preparing CF-ABS samples for tensile and flexural

tests, respectively. Figure 3 shows the dimensions of the test specimens used. The experiment is conducted in two sections: irradiated samples and irradiated filament. All irradiated ABS samples were printed using an entry-level 3D printer Makerbot Replicator 2x. Irradiated CF-ABS samples as well as samples made of irradiated CF-ABS and ABS filament were printed using Flashforge desktop 3D printer with a Hercules A2 hardened steel nozzle. Moreover, 100% infill and two perimeter layers were considered for the entire population. In addition, the ABS and CF-ABS filament was made using the same base ABS polymer (Sabic MG-94) and was manufactured by 3DXTech. The actual thickness and width of the samples were measured after irradiation and print using a caliper and minimum dimensions were recorded for calculations.

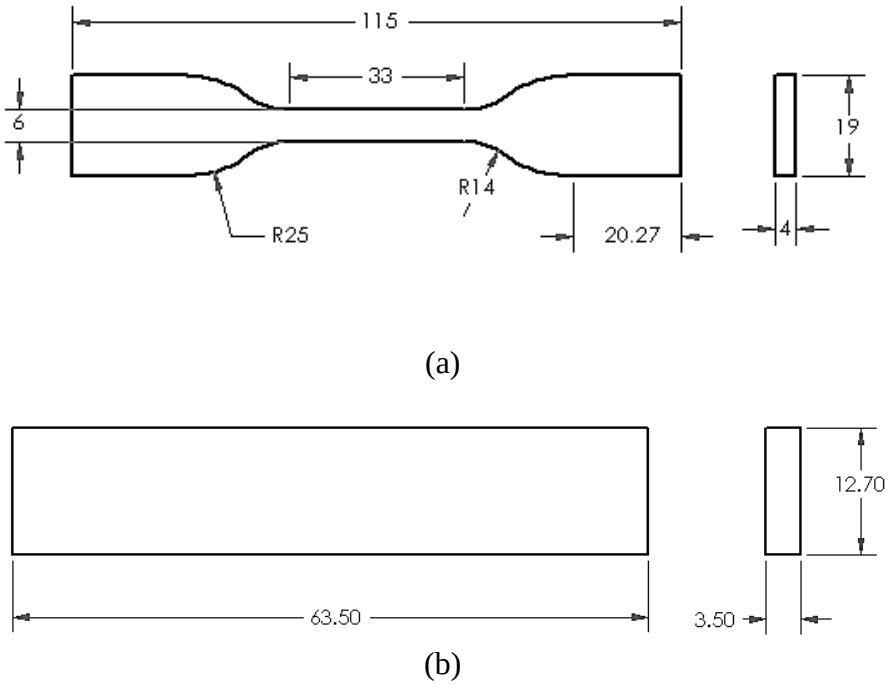

Fig. 3. (a) Tensile test specimens and (b) flexural test specimen (in mm).

Samples were irradiated using a Cobalt-60 gamma ray source. The radioactive decay of Cobalt-60 results in gamma rays with energies of 1173.2 keV and 1332.5 keV, which are sufficient to break chemical bonds but inadequate to produce artificial radioactivity. The doses used were categorized into two groups: low dose from 1 kGy to 15 kGy, and high dose with 1000 KGy, 1200 kGy and 1400 kGy. Six samples were tested at each dose for the irradiated samples experiments and four samples were tested for all irradiated filament experiments.

Tests were conducted using an MTS Insight 5 universal testing machine with a 5 kN load cell. An MTS extensometer with a gage length of 20 mm was used to measure the strain of tensile specimens. For flexural test, built-in LVDTs measured the displacement between the grips. For the ABS samples, pneumatic grips were displaced at rates of 5 mm/min and 1.2 mm/min for tensile and flexural tests respectively. For CF-ABS samples, a displacement rate of 2 mm/min and 1.2 mm/min was set for tensile and flexural tests respectively. ASTM D638 [18], D790 [19] and D3039 [20] testing procedures were followed for the entire set of tests. Finally, hardness testing was performed according to ASTM D2240 [21] using a portable Shore D indenter. Indentation was performed on the flexural test specimens before and after irradiation. To obtain consistent and repeatable results, all samples were indented on the surface where the first layer was deposited (the built plate side).

RESULTS AND DISCUSSION

ABS TEST RESULTS

Averaged tensile test results for irradiated samples (first scenario) are shown in Table 3, while the averaged flexural test results for the same samples are shown in Table 4. Averaged hardness test results are depicted in Table 5. Mechanical properties of samples were calculated using a custom MATLAB code (see appendix I and II). These properties include ultimate strength, elastic and flexural modulus and maximum elongation. The samples size for every test was 6. A first look at the results shows a significant loss in the ultimate strength and maximum elongation of samples for high doses. To better understand the degradation effects of gamma irradiation of samples, results are compared with data obtained from testing a controlled group of ABS samples fabricated with the exact same requirements. Results from the controlled group matches previous results obtained by others [22-26]. Based on the available data, it is concluded that for high dose group, tensile samples experienced nearly 74% loss of ultimate strength and almost 93% loss for their maximum elongation. Flexural samples lost 78% of their ultimate strength for high dose group and almost 92% of their maximum elongation. Flexural modulus increased by 23% for higher dose group, and elastic modulus increased by 25%. A slight increase (almost 13%) in the hardness of samples can be seen from the Shore D test results for the high dose group. On the other hand, considering ultimate strength, and maximum elongation obtained from both tests for low dose group, it can be concluded that samples did not experience more than 10% loss of property. Flexural and elastic modulus both increased by 17% and 5%, respectively. Finally, the hardness of samples irradiated at low dose increased by less than 5%. To better illustrate the effects

of gamma irradiation on the strength of material, some examples of the stress-strain curves, determined experimentally from tensile and flexural tests, are shown in Figures 4 and 5.

Table 3. Tensile test results for irradiated ABS samples

Treatments	Ultimate Strength (MPa)		Elastic Modulus (MPa)		Max. Elongation (%)	
	Mean	σ	Mean	σ	Mean	σ
Control	37.5	0.46	2001.7	35.27	6.19	2.25
1 kGy	38.2	0.46	2110.4	41.34	7.66	2.09
3 kGy	38.0	0.76	2086.6	84.28	7.75	4.38
5 kGy	38.0	0.36	2064.1	26.44	7.83	1.32
7 kGy	38.2	0.25	2086.4	56.72	7.32	4.94
10 kGy	38.6	0.72	2142.4	47.38	6.77	2.28
15 kGy	38.8	0.48	2184.7	67.49	6.62	3.81
1000 kGy	10.8	1.11	2447.9	169.11	0.57	0.25
1200 kGy	10.0	0.73	2501.8	240.97	0.46	0.46
1400 kGy	8.1	0.49	2537.3	261.03	0.34	0.12

Table 4. Flexural test results for irradiated ABS samples

Treatments	Ultimate Strength (MPa)		Flexure Modulus (MPa)		Max. Elongation (%)	
	Mean	σ	Mean	σ	Mean	σ
Control	52.1	1.76	1715.5	65.72	7.58	1.03
1 kGy	58.9	4.82	1927.8	83.25	8.24	0.75
3 kGy	58.7	1.10	1931.3	70.71	8.10	0.60
5 kGy	59.8	0.86	2061.1	66.85	7.76	0.80
7 kGy	59.8	1.17	2054.7	47.46	7.70	0.72
10 kGy	59.7	2.71	2039.5	130.29	7.78	0.89
15 kGy	60.5	1.76	2045.6	70.06	7.10	1.16
1000 kGy	12.0	0.82	2062.4	116.61	0.89	0.45
1200 kGy	11.7	0.65	2059.6	86.88	0.56	0.04
1400 kGy	11.0	0.74	2230.7	147.21	0.49	0.02

Table 5. Hardness test results for irradiated ABS samples

Treatments	Shore D	
	Mean	σ
Control	76.4	1.57
1 kGy	77.1	0.84
3 kGy	77.8	0.55
5 kGy	80.3	0.63
7 kGy	79.2	0.62
10 kGy	77.5	1.47
15 kGy	80.3	0.63
1000 kGy	84.3	0.85
1200 kGy	84.8	0.95
1400 kGy	85.8	0.63

It is worth mentioning that the effects of irradiation on the high dose group was so severe that a proper stress strain curve could not be obtained from any of the test results.

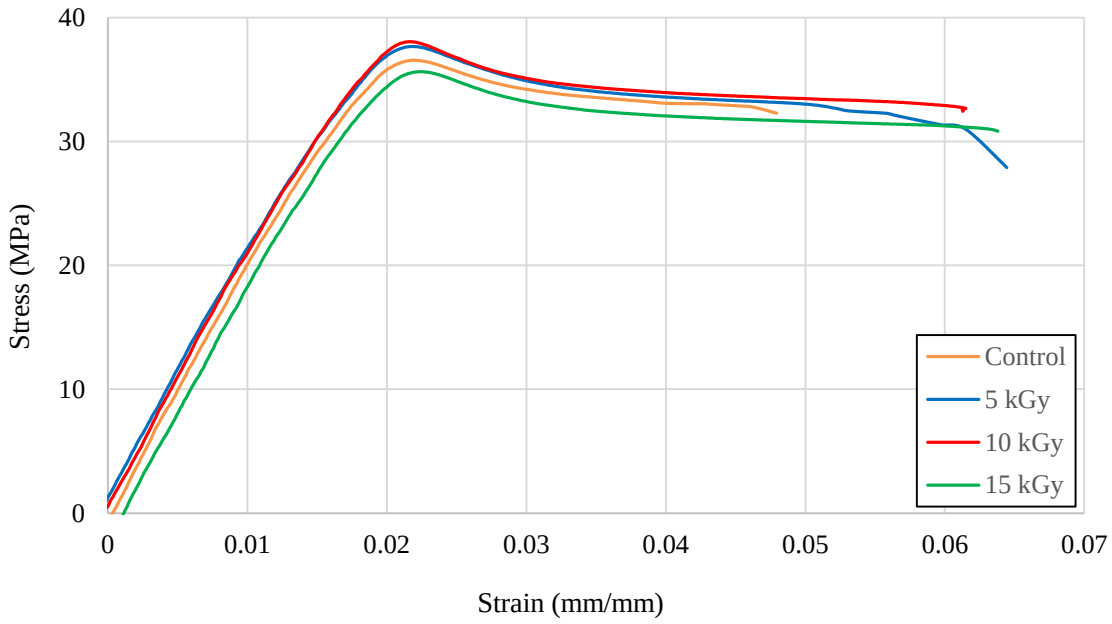

Fig. 4. Stress-strain curves for irradiated ABS sample, obtained from tensile tests.

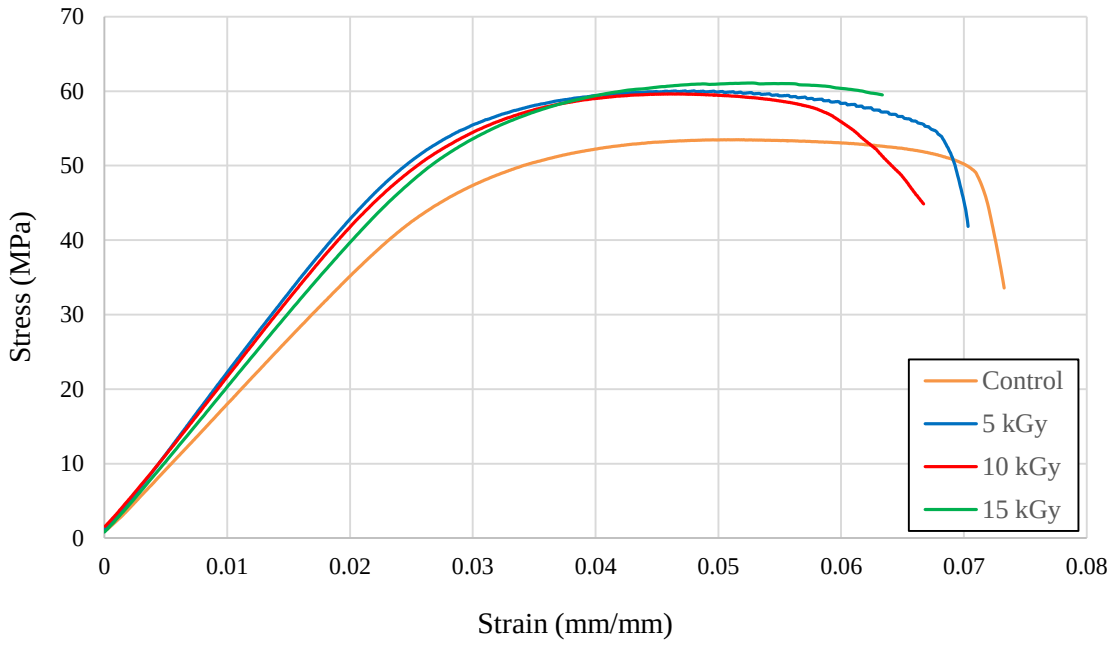

Fig. 5. Stress-strain curves for irradiated ABS sample, obtained from flexural tests.

In the second scenario, the same types of testing were conducted on samples made using irradiated filament. This round of testing will determine whether the FDM technology and the materials being tested are suitable for gaining earth independency. Tensile, flexural and hardness test results are presented in Tables 6, 7 and 8, respectively. It should be noted that since the high dose group lost more than 70% of its mechanical properties, as a result it became almost impossible to print any samples from the group without significant modification of the printers' extruders and settings. Since the purpose of this study is taking advantage of the FDM 3D printer that is already operational onboard the ISS with as little astronaut labor required as possible, the high dose group was disqualified from further testing and analysis. Based on the trial and error, it can be concluded that filaments that are exposed to 800 kGy of gamma radiation and higher will not be printable without altering the mechanisms and settings of the printer. The same

justification can be made for CF-ABS by considering the inherent brittleness of CF-ABS due to existence of short carbon fibers in the filament.

Table 6. Tensile test results for irradiated ABS filament

Treatments	Ultimate Strength (MPa)		Elastic Modulus (MPa)		Max. Elongation (%)	
	Mean	σ	Mean	σ	Mean	σ
Control	37.5	0.46	2001.7	35.27	6.19	2.25
1 kGy	37.3	0.62	2036.1	44.17	3.48	0.61
3 kGy	38.0	0.52	2124.9	60.86	4.41	0.63
5 kGy	39.2	0.33	2151.4	32.13	4.18	0.31
7 kGy	39.0	0.34	2079.0	32.56	4.08	0.53
10 kGy	39.0	0.32	2076.8	21.98	2.04	1.16
15 kGy	39.1	0.73	2082.8	36.89	3.44	1.03

Table 7. Flexural test results for irradiated ABS filament

Treatments	Ultimate Strength (MPa)		Flexure Modulus (MPa)		Max. Elongation (%)	
	Mean	σ	Mean	σ	Mean	σ
Control	52.1	1.76	1715.5	65.72	7.58	1.03
1 kGy	54.0	2.42	1674.2	124.50	8.08	0.92
3 kGy	57.7	1.45	1773.3	39.48	7.89	0.36
5 kGy	59.2	0.64	1872.1	10.21	8.01	0.80
7 kGy	59.3	0.33	1856.2	17.94	8.15	0.55
10 kGy	55.9	1.36	1792.6	55.34	7.16	0.63
15 kGy	53.9	2.26	1673.5	130.84	8.69	1.08

The first look at the tensile test results reveals that the ultimate strength increased by almost 4% as the dosage increased from 1 kGy to 15 kGy. Also, it seems like the elastic modulus behavior is indeterminate by the increase or decrease of dosage. Finally, the maximum elongation decreased by almost 56% as the dosage increased. Flexural test results indicate a 3% increase in the ultimate strength with an increase in the

dosage which conforms to the results obtained from the tensile test results. Flexural modulus increased first then started to decrease as the dosage increased. Maximum elongation showed no significant change throughout the test. Stress-strain curves for ABS filament obtained from the flexural tests are presented in Figures 6 and 7 for visual comparison of the results.

Table 8. Hardness test results for irradiated ABS filament

Treatments	Shore D	
	Mean	σ
Control	76.4	1.57
1 kGy	69.0	3.00
3 kGy	74.4	1.08
5 kGy	75.1	0.89
7 kGy	75.4	0.82
10 kGy	71.0	2.15
15 kGy	69.5	0.87

The first look at the tensile test results reveals that the ultimate strength increased by almost 4% as the dosage increased from 1 kGy to 15 kGy. Also, it seems like the elastic modulus behavior is indeterminate by the increase or decrease of dosage. Finally, the maximum elongation decreased by almost 56% as the dosage increased. Flexural test results indicate a 3% increase in the ultimate strength with an increase in the dosage which conforms to the results obtained from the tensile test results. Flexural modulus increased first then started to decrease as the dosage increased. Maximum elongation showed no significant change throughout the test. Stress-strain curves for ABS filament obtained from the flexural tests are presented in Figures 6 and 7 for visual comparison of the results.

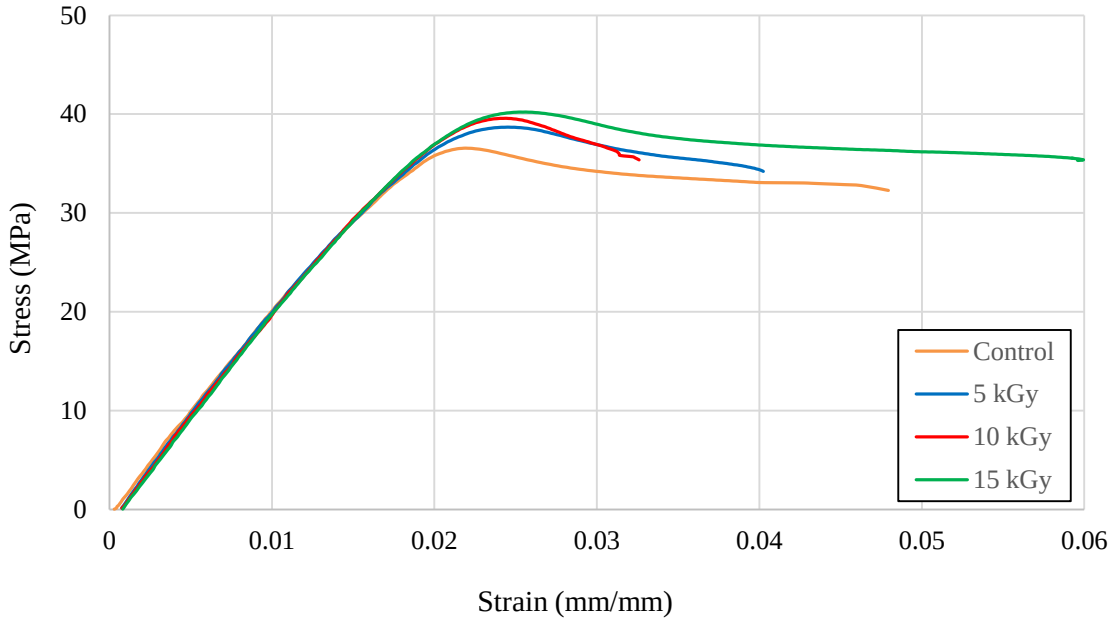

Fig. 6. Stress-strain curves for irradiated ABS filament, obtained from tensile tests.

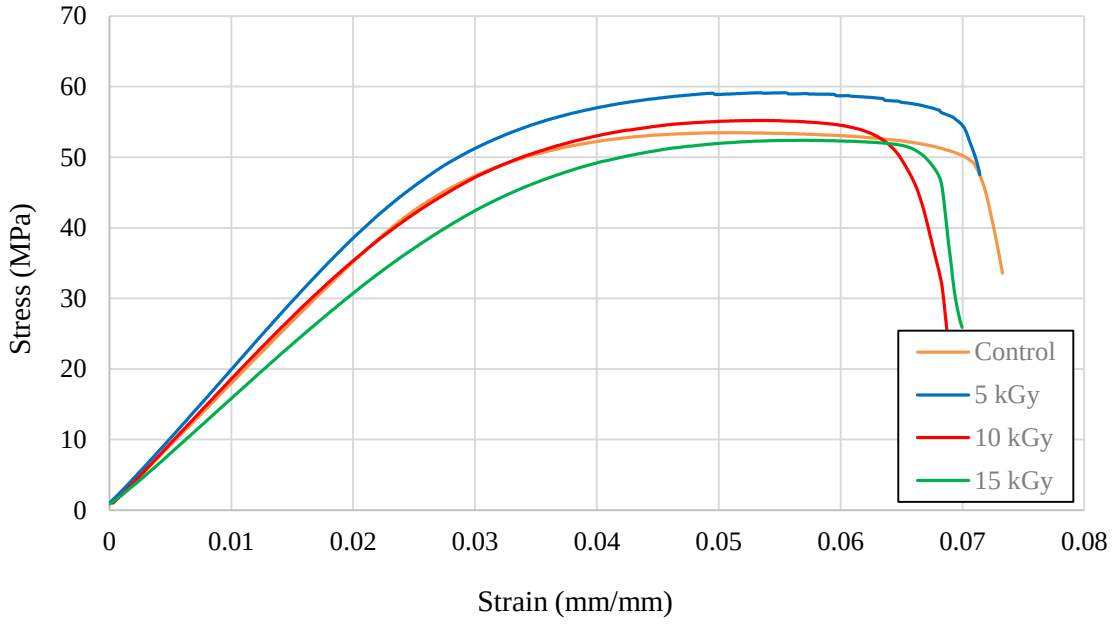

Fig. 7. Stress-strain curves for irradiated ABS filament, obtained from flexural tests.

By comparing the curves and the obtained results, it can be concluded that low dose group became stronger but more brittle, while the high dose group suffered from

severe loss of mechanical strength as well as substantial brittleness. This can be explained by considering the interaction of gamma rays with polymers like ABS. Gamma radiation can produce extremely reactive unpaired electrons which result in irreversibly broken covalent bonds. These unpaired electrons exist in free radical or chemical species that are a product of irradiation and their chemical reactions in polymers can cause crosslinking between polymer chains, chain scission or oxidations of carbon chains. These chemical reactions can alter the bonds between the atoms of the polymer strand which can result in a change of chemical and mechanical properties of a polymer [27]. Figure 8 shows samples after exposure to gamma rays. As can be seen, samples exposed to low doses exhibit almost no change in their appearance, while samples exposed to high doses went through extreme color transformation. Figure 9 shows ABS samples made of irradiate filament. The only visible color change was observed for filament exposed to 15 kGy of gamma radiation. Lower doses caused no noticeable change in the appearance of the samples.

(a)

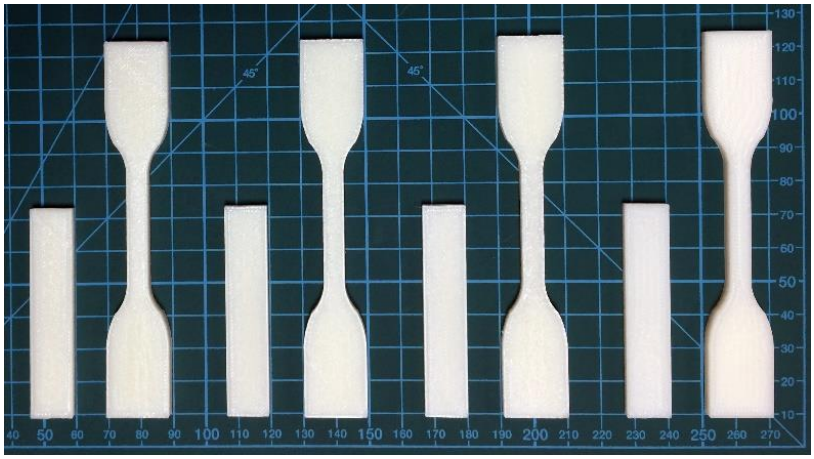

(b)

Fig. 8. Tensile and flexural test specimens before and after irradiation by gamma rays. (a) From right to left: control sample, samples exposed to 1000 kGy, 1200 kGy and 1400 kGy. (b) From right to left: control sample, samples exposed to 1 kGy, 5 kGy and 10 kGy.

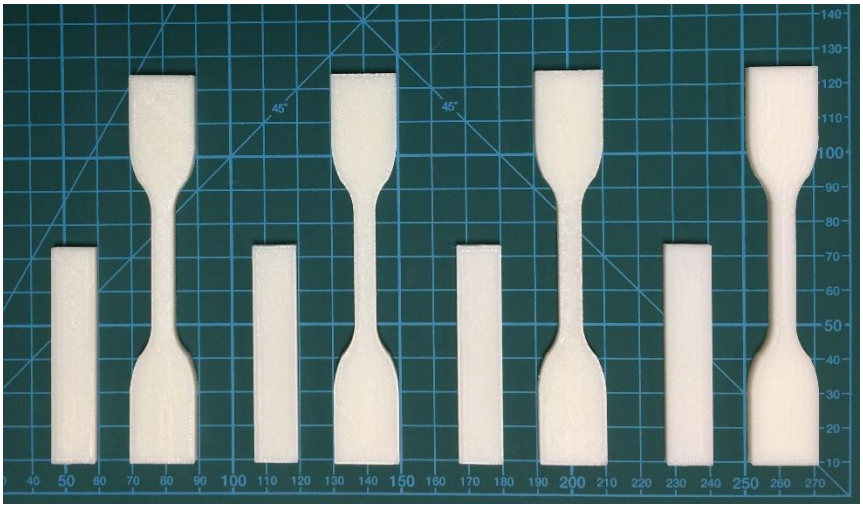

Fig. 9. Tensile and flexural test specimens made of irradiated ABS filament. From right to left: control sample, samples exposed to 1 kGy, 5 kGy and 10 kGy.

Figures 10, 11 and 12 enable us to graphically compare the results from irradiated samples and filaments followed by statistical analysis of the results to determine whether the samples made of irradiated ABS filament can have the same mechanical performance as the irradiated samples. Graphical comparison of the tensile test results shows almost

no significant change in the ultimate strength and elastic modulus of the samples. On the other hand, a significant decrease of maximum elongation is evident which suggests an increase in the brittleness of the material. Figure 11 suggests a slight decrease in the flexural modulus of the samples. However, the ultimate strength and maximum elongation remained almost constant. Finally, surface hardness of samples made of irradiated filament seem to have decreased. Statistical analysis will determine whether these differences are of any significance.

ABS STATISTICAL ANALYSIS

All pairs Tukey-Kramer analyses were performed to attain a conclusive comparison of mechanical properties obtained through the aforementioned tests for ABS samples printed by irradiated filament and those irradiated after being printed. All of these analyses were carried out at 95% confidence level. The mean values are compared considering the contribution of all dosages. First, the means of ultimate stresses acquired from tensile tests were compared and it was found that with an infinitesimal p-value, the mean response for irradiated samples is significantly lower by 1.471 MPa than that of the samples printed by irradiated filament. Means of elastic moduli were compared with a difference of 1.608 MPa and an adjusted p-value of 0.993, which indicates that this difference is absolutely insignificant and thus the elastic modulus would be the same for both cases. Finally, the means of maximum elongations were compared and it was shown that irradiated samples have a 5.092-unit larger mean of maximum elongations, with an infinitesimal p-value, which makes this difference significant.

(a)

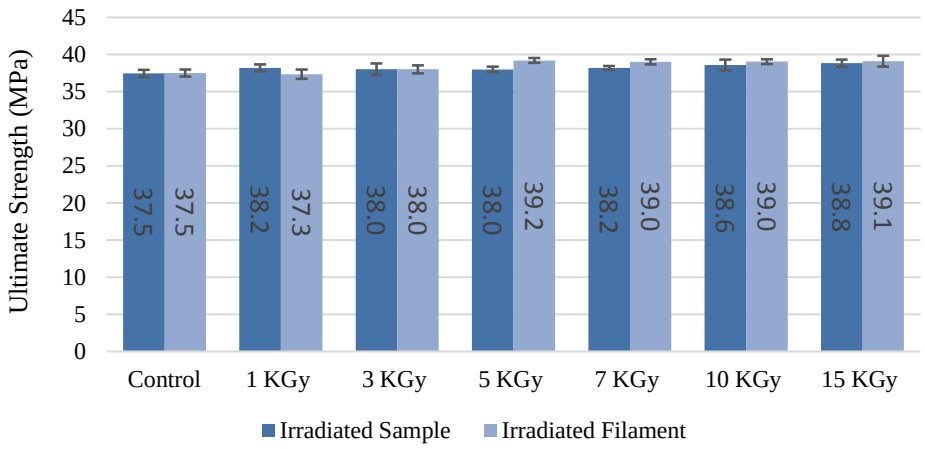

(b)

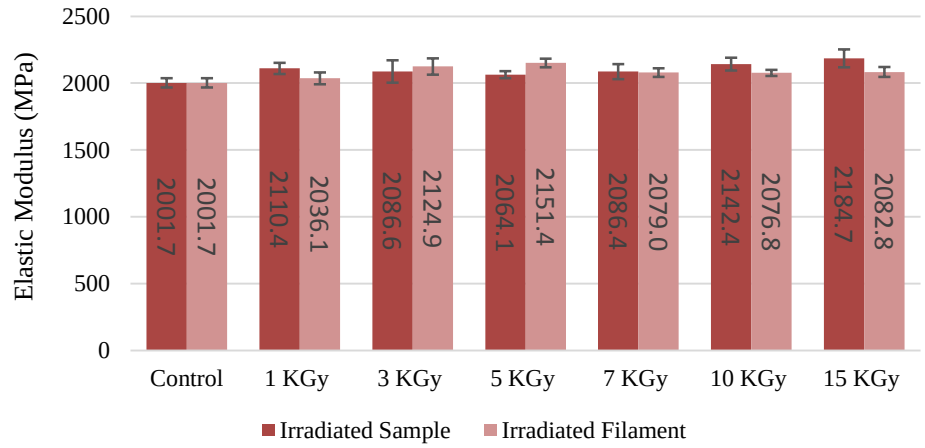

(c)

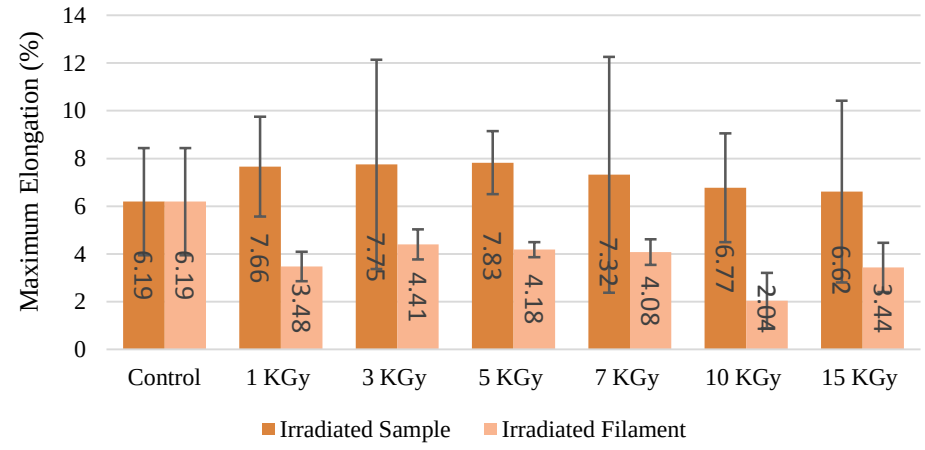

Fig. 10. Graphical comparison of tensile test results for ABS samples. (a) ultimate strength, (b) elastic modulus and (c) maximum elongation.

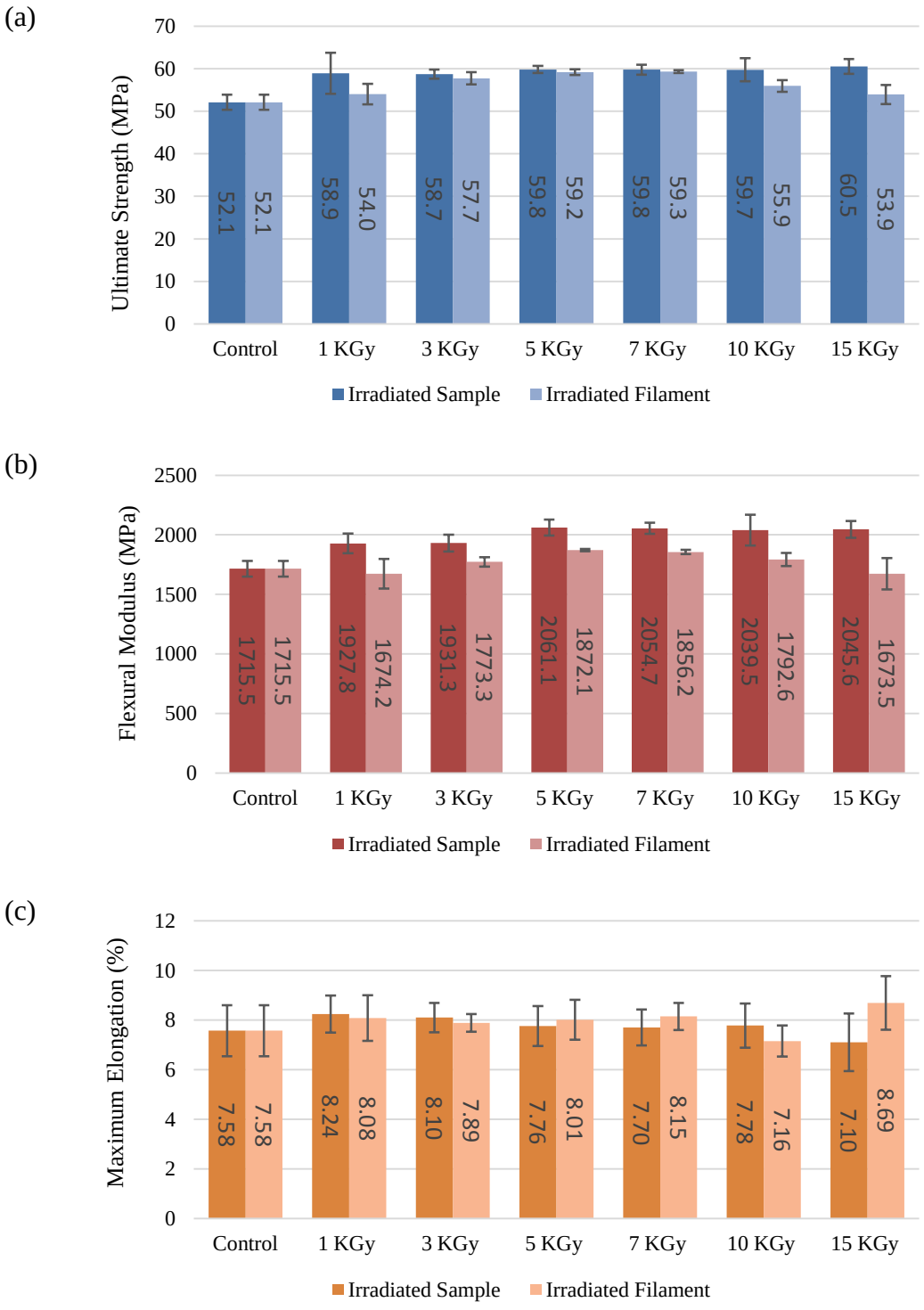

Fig. 11. Graphical comparison of flexural test results for ABS samples. (a) ultimate strength, (b) flexural modulus and (c) maximum elongation.

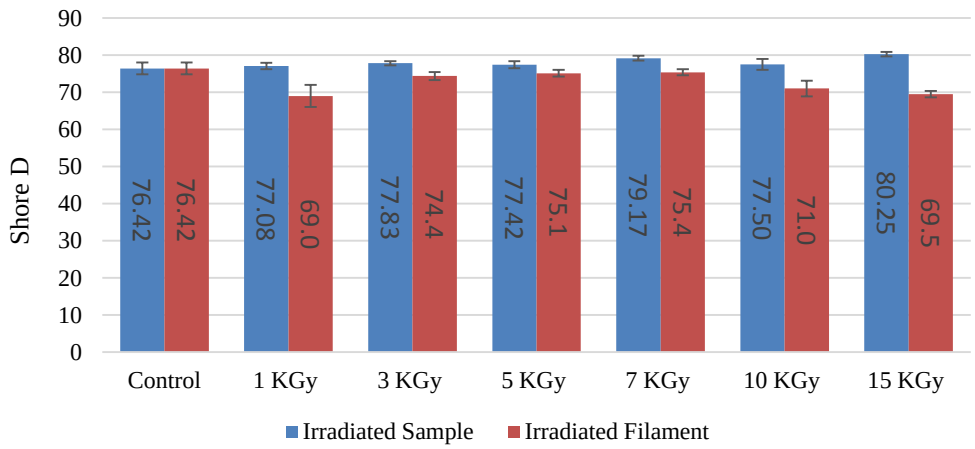

Fig. 12. Graphical comparison of surface hardness for ABS samples

The mean ultimate stress of the irradiated samples measured by flexural tests was found to be higher by 2.895 MPa than the one belonging to irradiated filament. This difference was considered significant, as the adjusted p-value was equal to 0.000078. The mean of flexural moduli for irradiated samples proved to be significantly higher by an infinitesimal p-value and a major difference of 196.856 MPa from its counterpart. As for the means of maximum elongations, although the difference was just 0.655 units in favor of the irradiated samples, by a 95% confidence level and a significance factor of 0.05, the adjusted p-value of 0.0259166 led to a conclusion of significant difference between the means.

In the last analysis, the means of hardness values for the two types of samples were compared, which showed that the irradiated samples have a mean hardness which is 5.813 units more than that of the irradiated filament. This difference was found to be significant by an infinitesimal p-value.

CF-ABS TEST RESULTS

CF-ABS test results are presented in the same manner as ABS. Averaged tensile test results for irradiated CF-ABS samples are shown in table 9, while the averaged flexural test results for the same samples are shown in table 10. Averaged hardness test results are depicted in table 11. The samples size for every test was four. Unlike the regular ABS, results show a slight increase in the ultimate strength and elastic modulus. On the other hand, maximum elongation decreases significantly. Considering the ultimate strength resulted from both tests, it can be concluded that samples did not experience more than 10% change. Flexural and elastic moduli resulted from both tests seem to fluctuate within 15% of the minimum and maximum values. Further statistical analysis is needed to determine the significance of any changes. Finally, the hardness of samples decreased by 3%. To better illustrate the effects of gamma irradiation on the strength of material, some examples of the stress-strain curves, determined experimentally from tensile and flexural tests, are shown in figures 13 and 14.

Table 9. Tensile test results for irradiated CF-ABS samples

Treatments	Ultimate Strength (MPa)		Elastic Modulus (MPa)		Max. Elongation (%)	
	Mean	σ	Mean	σ	Mean	σ
Control	32.6	1.07	3554.3	145.93	4.55	1.31
1 kGy	32.7	0.60	3608.4	114.90	4.24	1.00
3 kGy	32.1	0.22	3583.3	133.59	4.55	1.92
5 kGy	33.8	0.83	3696.7	219.61	2.11	0.25
7 kGy	33.1	0.38	3731.4	146.31	1.75	0.23
10 kGy	33.5	0.55	3733.2	141.41	1.83	0.12
15 kGy	33.4	0.68	3643.3	139.75	1.79	0.15

Table 10. Flexural test results for irradiated CF-ABS samples

Treatments	Ultimate Strength (MPa)		Flexure Modulus (MPa)		Max. Elongation (%)	
	Mean	σ	Mean	σ	Mean	σ
Control	62.3	1.27	2847.7	73.97	4.8	0.46
1 kGy	62.5	0.96	2826.7	84.81	5.1	0.45
3 kGy	60.6	0.89	2769.6	72.63	5.0	0.56
5 kGy	62.3	1.15	2841.0	77.19	4.9	0.29
7 kGy	61.3	0.77	2703.9	65.97	4.9	0.32
10 kGy	63.2	0.85	2746.0	69.22	5.0	0.21
15 kGy	60.7	0.67	2665.6	106.34	5.1	0.40

Table 11. Hardness test results for irradiated CF-ABS samples

Treatments	Shore D	
	Mean	σ
Control	79.50	0.58
1 kGy	78.33	0.24
3 kGy	76.92	0.45
5 kGy	78.92	0.73
7 kGy	77.33	0.47
10 kGy	77.83	0.75
15 kGy	77.33	0.80

In the second scenario, same types of testing was conducted on samples made of irradiated CF-ABS filament. Tensile, flexural and hardness test results are presented in tables 12, 13 and 14, respectively. The first look at the tensile test results reveals a disorganized behavior by the material. The ultimate strength and elastic and flexure moduli do not follow any ascending or descending paths by the increase in the dosage, except for the initial decrease in the flexural modulus and ultimate strength when

compared to the control sample for flexural tests. Finally, the maximum elongation resulted from tensile tests decreased by almost 37% as the dosage increased. Maximum elongation remained constant on average throughout the flexural test. Stress-strain curves for CF-ABS filament obtained from both tests are presented in figures 15 and 16 for visual comparison of the results.

By comparing the curves and the obtained results, it can be concluded that samples were more vulnerable to flexural tests than tensile tests. Although there are signs of brittleness in the results, they are not evident enough to be able to draw any strong conclusions. Statistical analysis will determine the conclusive effects of gamma irradiation on the mechanical performance of the material. Unlike regular ABS samples, CF-ABS samples showed no visible change in their appearance, this is in part due to their natural color (black) that is less prone to show slight color changes.

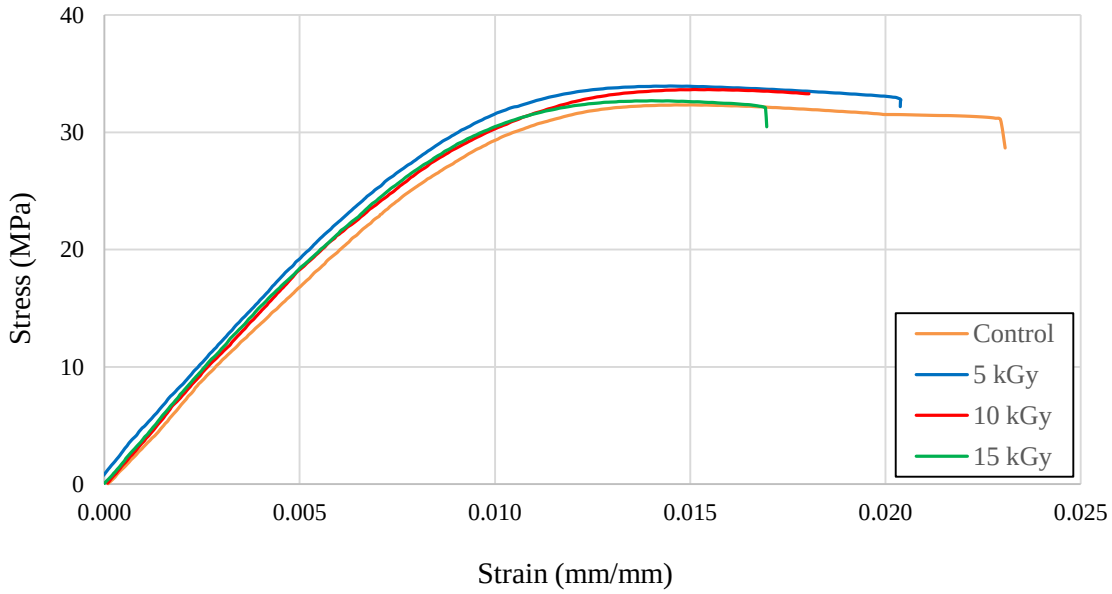

Fig. 13. Stress-strain curves for irradiated CF-ABS sample, obtained from tensile tests.

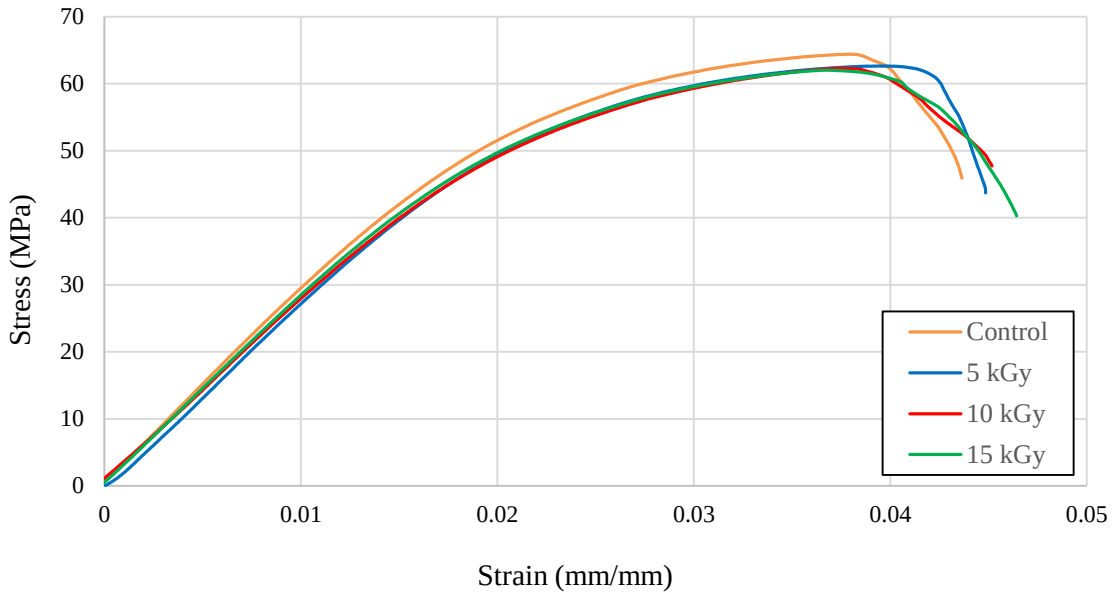

Fig. 14. Stress-strain curves for irradiated CF-ABS sample, obtained from flexural tests.

Table 12. Tensile test results for irradiated CF-ABS filament

Treatments	Ultimate Strength (MPa)		Elastic Modulus (MPa)		Max. Elongation (%)	
	Mean	σ	Mean	σ	Mean	σ
Control	32.6	1.07	3554.3	145.93	4.55	1.31
1 kGy	30.7	0.47	3722.5	472.49	2.47	0.31
3 kGy	33.5	2.11	3945.8	287.41	1.78	0.50
5 kGy	31.6	0.56	3842.4	547.64	1.42	0.37
7 kGy	33.9	0.29	3795.7	72.96	1.82	0.22
10 kGy	31.2	0.12	3651.6	134.40	1.43	0.13
15 kGy	33.4	0.20	3818.0	126.72	1.70	0.19

Table 13. Flexural test results for irradiated CF-ABS filament

Treatments	Ultimate Strength (MPa)		Flexure Modulus (Mpa)		Max. Elongation (%)	
	Mean	σ	Mean	σ	Mean	σ
Control	62.3	1.27	2847.7	73.97	4.8	0.46
1 kGy	50.5	1.19	2279.2	111.76	4.5	0.26
3 kGy	51.7	1.32	2347.3	116.62	4.2	0.16
5 kGy	49.8	0.57	2287.2	46.80	4.6	0.14
7 kGy	52.4	0.77	2353.3	66.88	4.8	0.20
10 kGy	49.0	0.81	2323.7	65.97	4.5	0.26
15 kGy	51.4	0.60	2364.7	56.60	4.5	0.31

Table 14. Hardness test results for irradiated CF-ABS filament

Treatments	Shore D	
	Mean	σ
Control	79.50	0.58
1 kGy	73.00	1.38
3 kGy	73.63	0.96
5 kGy	70.25	0.25
7 kGy	72.00	0.79
10 kGy	72.88	0.54
15 kGy	73.63	1.14

Similar to ABS, figures 17, 18 and 19 are to graphically compare the results from irradiated samples and filaments followed by statistical analysis. Comparison of tensile test results show no significant difference between irradiated sample and irradiated filament in terms of ultimate strength and elastic modulus. However, for maximum elongation, a noticeable difference can be seen for samples exposed to 1, 3 and 5 kGy of radiation. Results are somewhat different for flexural tests. Both ultimate strength and flexural modulus are lower compared to their counterparts. In case of ultimate strength, irradiated filament is 20% weaker than irradiated samples. For flexural modulus, results

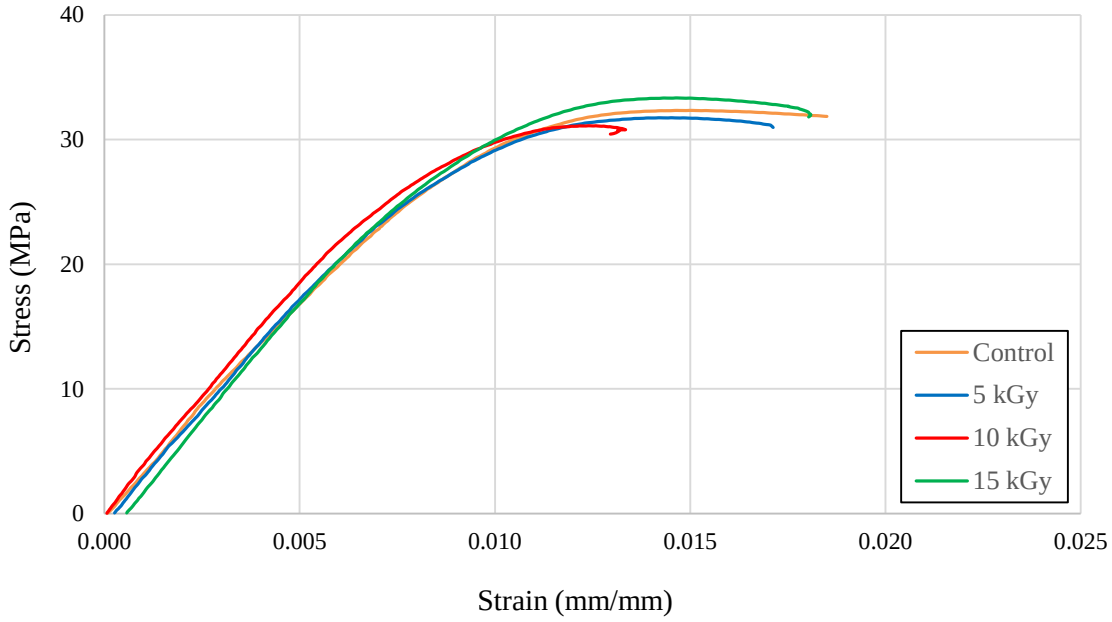

Fig. 15. Stress-strain curves for irradiated CF-ABS filament, obtained from tensile tests.

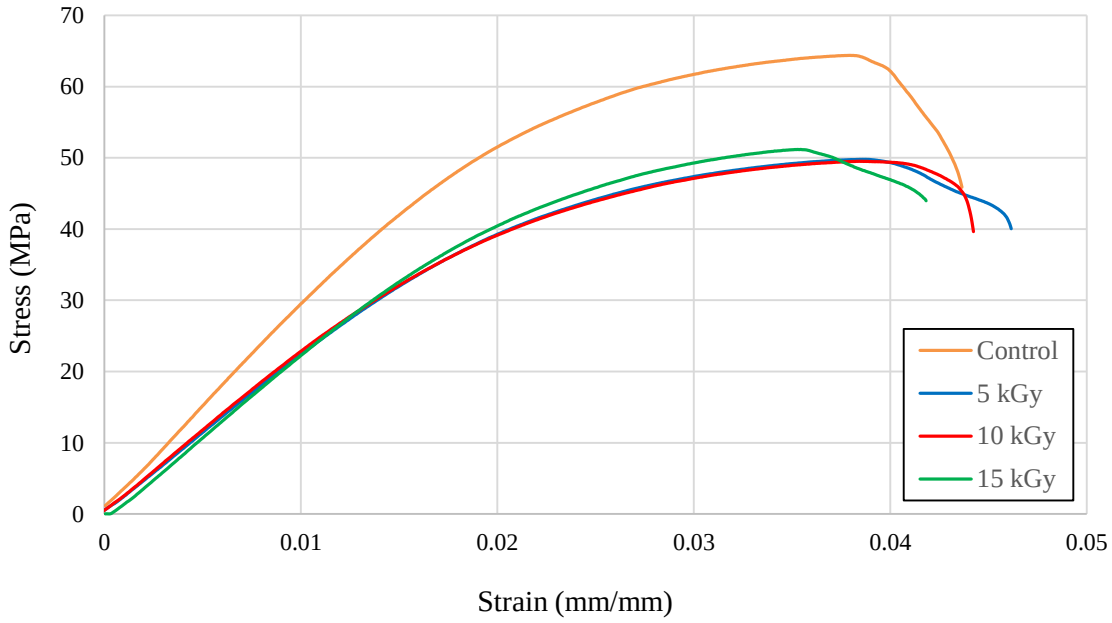

Fig. 16. Stress-strain curves for irradiated CF-ABS filament, obtained from flexural tests.

show 14% decrease on average for each dosage. In both tests the maximum elongation for samples made of irradiated filament is lower than irradiated samples. Finally, surface hardness of samples made of irradiated filament seem to have decreased, similar to regular ABS. Statistical analysis will determine whether these differences are of any significance.

CF-ABS STATISTICAL ANALYSIS

All pairs Tukey-Kramer analyses were also carried out for the test results of carbon fiber ABS samples of the two types (irradiated samples and irradiated filament), in a manner similar to that of ABS comparisons. It was found that with an adjusted p-value of 0.0213673, the mean response for irradiated samples is significantly higher by 0.645 MPa than that of the samples printed by irradiated filament. Means of elastic moduli had a difference of -99.441 MPa and an adjusted p-value of 0.2248185, which is an indication of insignificant difference and thus the elastic modulus can be considered the same for both cases. Means of maximum elongations were compared and it was shown that irradiated samples had a 0.916-unit larger mean of maximum elongations with a large p-value of 0.5047858, rendering this small difference as insignificant and negligible. It was concluded that both types of samples have the same maximum elongation mean.

Mean ultimate stress of the irradiated samples obtained from flexural tests was found to be higher by 10.987 MPa than the one belonging to the other sample type. This difference was considered as significant, as the adjusted p-value was infinitesimal. The means of flexural moduli for irradiated samples proved to be significantly higher by an

infinitesimal p-value and a major difference of 434.767 MPa from its counterpart. Maximum elongations for the irradiated samples had a mean which was found to be 0.446 units higher than that of the other type of samples. This difference was found to be significant, with an adjusted p-value of 0.0001316.

Finally, the means of hardness values for the two types of samples were compared. The results of the analysis suggested that the irradiated samples have a mean hardness which is 5.198 Shore D more than that of the other type of samples. The infinitesimal p-value proved this difference to be significant.

It is fair to state that ABS samples exposed to high doses (1000-1400 kGy) showed significant degradation in their mechanical properties, while samples exposed to low doses (1 – 15 kGy) maintained their mechanical integrity. For CF-ABS samples, the mechanical properties of samples are highly dependent on fibers' length and orientation [28] therefore addressing the cause or causes of changes in mechanical performance of the material requires further investigation on effects of irradiation on fiber orientation of CF-ABS samples which is out of the scope of this study. Based on the data provided in Tables 1 and 2, samples fabricated out of ABS and CF-ABS using FDM technique can be used in LEO, on board the ISS and on the surface of Mars for long periods of time without any significant loss of mechanical properties due to exposure to gamma radiation. Moreover, results showed that ABS and CF-ABS in filament form can also be stored as feedstock supply for long duration space missions without jeopardizing printability or mechanical performance.

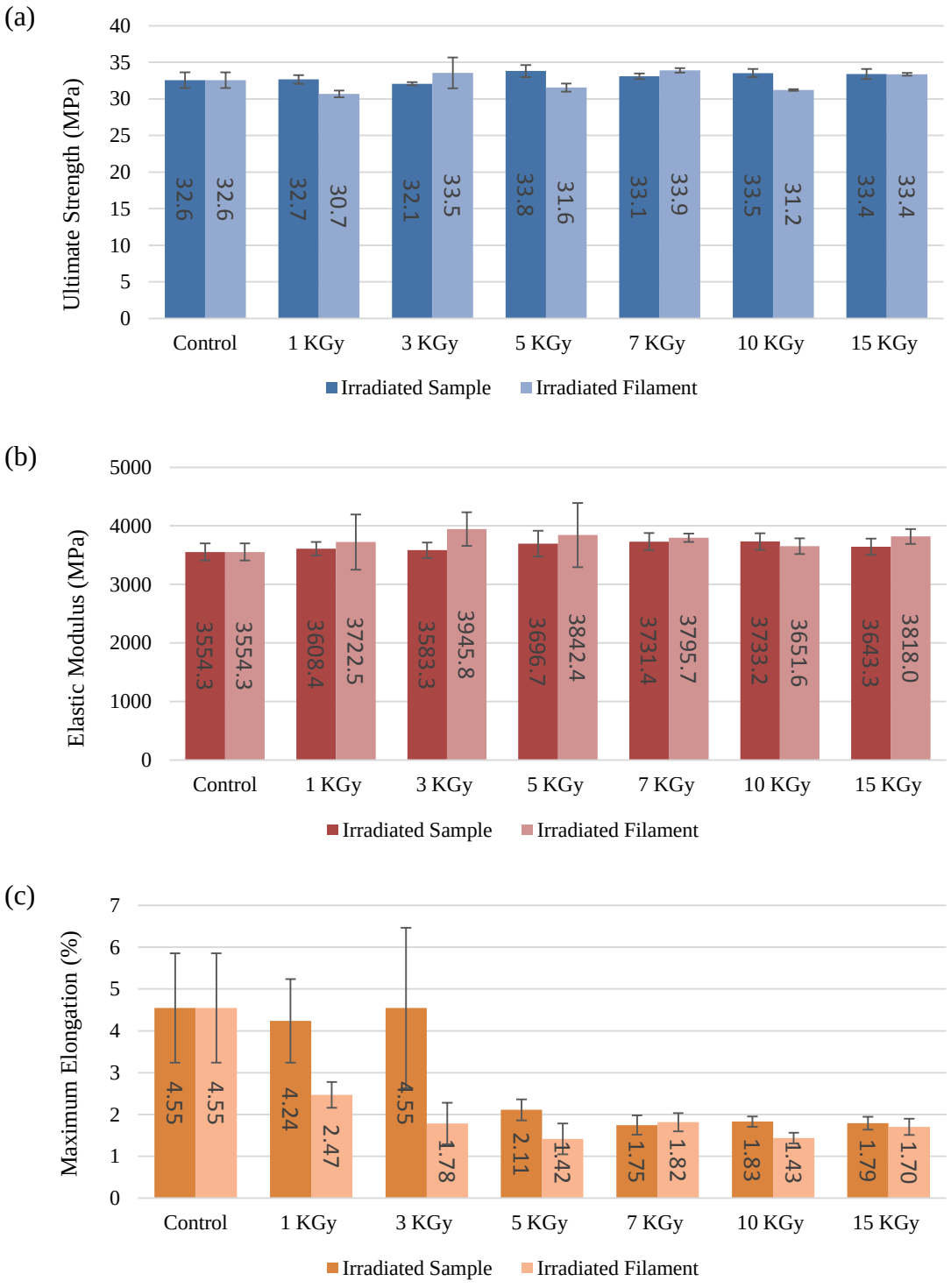

Fig. 17. Graphical comparison of tensile test results for CF-ABS samples. (a) ultimate strength, (b) elastic modulus and (c) maximum elongation.

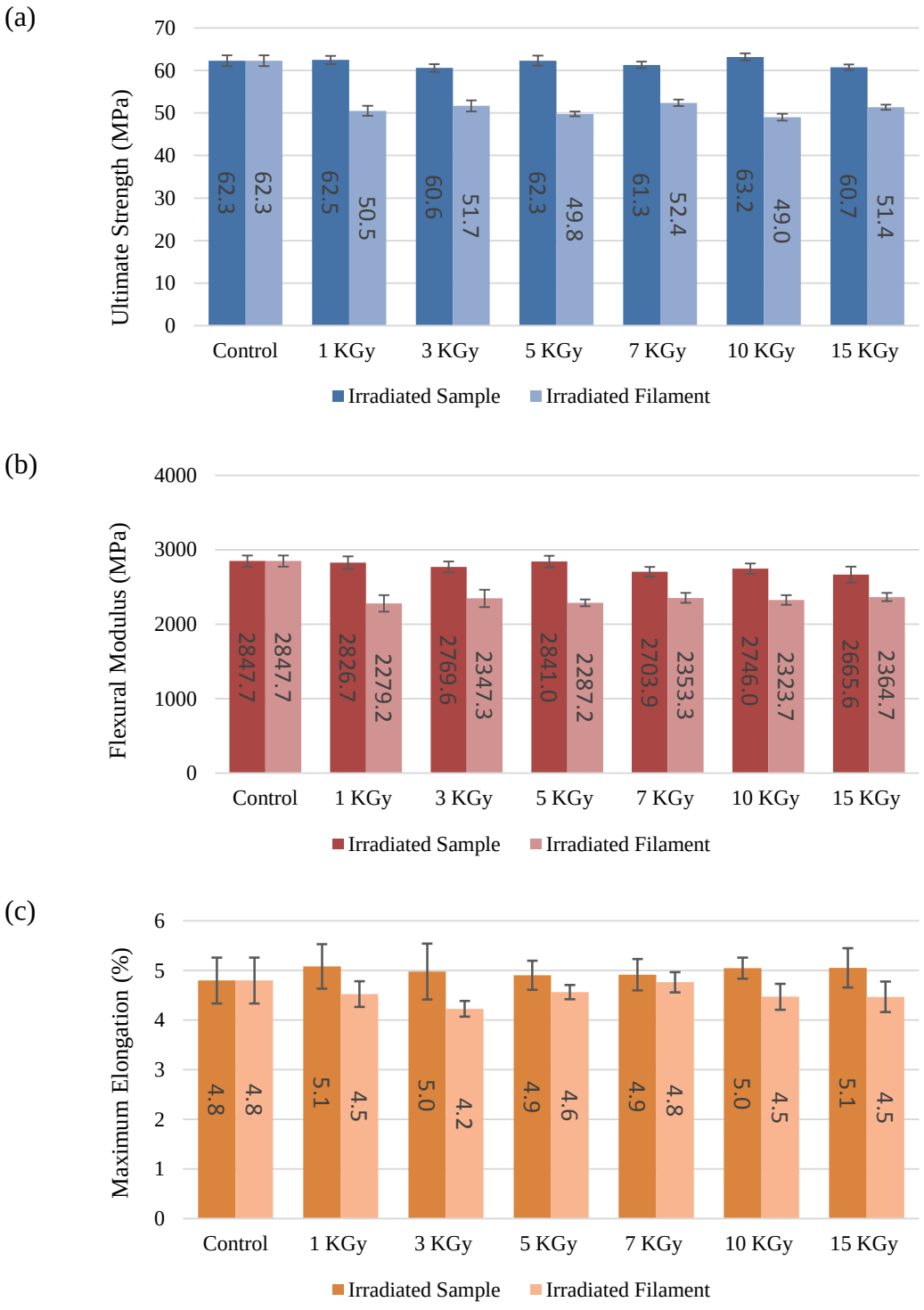

Fig. 18. Graphical comparison of flexural test results for CF-ABS samples. (a) ultimate strength, (b) flexural modulus and (c) maximum elongation.

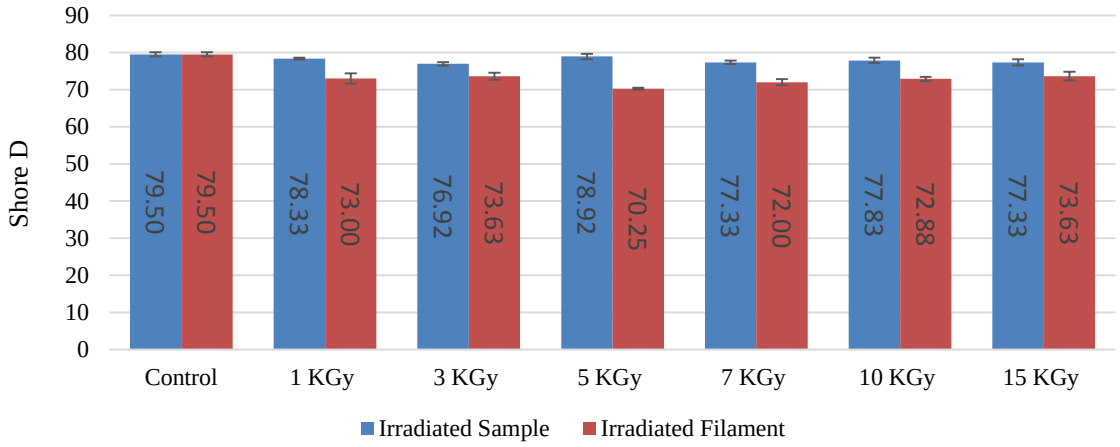

Fig. 19. Graphical comparison of surface hardness for ABS samples

CONCLUSION

ABS and CF-ABS were exposed to gamma irradiation in two different forms; filament and samples fabricated using FDM technique. Two dose groups (low dose: 1 to 15 kGy, and high dose: 1000, 1200 and 1400 kGy) were chosen to simulate space radiation environment. Samples showed significant loss of mechanical properties at high doses and negligible loss at low doses. Overall, irradiation caused the brittleness of ABS and CF-ABS samples to increase. This conclusion is based on the increase of ultimate strength and hardness, and the decrease of maximum elongation for low dose group (ABS in particular). Since the simulated irradiation doses for low dose group are the equivalent of exposure to space radiation over a prolong space mission, it can be concluded that parts fabricated using FDM technology can safely be used on board the ISS, in deep space and on future mars or moon missions without any concern for failure due to degradation caused by gamma radiation.

More mechanical and chemical testing should be done to further understand the behavior of 3D printed parts when exposed to radiation. Furthermore, different thermoplastics should also be considered for these tests to be able to expand the possibilities of in-space manufacturing.

REFERENCES

[1] Wohler's Associates, "Wohler's Report, 3D Printing and Additive Manufacturing State of the Industry, Annual Worldwide Progress Report", (2014): 16-17.

[2] Cucinotta, Francis A., and Marco Durante. "Cancer risk from exposure to galactic cosmic rays: implications for space exploration by human beings." Lancet Oncol. 7 (2006): 431-35.

[3] Townsend, Lawrence W. "Implications of the space radiation environment for human exploration in deep space." Radiation protection dosimetry 115.1-4 (2005): 44-50.

[4] Cucinotta, Francis A., et al. "Radiation dosimetry and biophysical models of space radiation effects." Gravitational and Space Biology 16.2 (2003): 11-19.

[5] Badhwar, G. D., et al. "Space radiation absorbed dose distribution in a human phantom." Radiation research 157.1 (2002): 76-91.

[6] Cucinotta, Francis A., et al. "Space radiation cancer risks and uncertainties for Mars missions." Radiation research 156.5 (2001): 682-688.

[7] Grossman, E., and I. Gouzman. "Space environment effects on polymers in low earth orbit." Nuclear Instruments and Methods in Physics Research Section B: Beam Interactions with Materials and Atoms 208 (2003): 48-57.

[8] Harrison, Courtney, et al. "Polyethylene/boron nitride composites for space radiation shielding." Journal of applied polymer science 109.4 (2008): 2529-2538.

[9] Rochus, Pierre, et al. "New applications of rapid prototyping and rapid manufacturing (RP/RM) technologies for space instrumentation." Acta Astronautica 61.1 (2007): 352-359.

[10] Beyer, Christiane. "Strategic implications of current trends in additive manufacturing." Journal of Manufacturing Science and Engineering 136.6 (2014): 064701.

[11] Guo, Nannan, and Ming C. Leu. "Additive manufacturing: technology, applications and research needs." Frontiers of Mechanical Engineering 8.3 (2013): 215-243.

[12] Snyder, Michael, Jason Dunn, and Eddie Gonzalez. "The effects of microgravity on extrusion based additive manufacturing." Proceedings of the AIAA SPACE Conference and Exposition. 2013.

[13] Hoyt, Robert P., et al. "SpiderFab: An architecture for self-fabricating space systems." AIAA SPACE 2013 Conference and Exposition. 2014.

[14] Benton, E. R., and E. V. Benton. "Space radiation dosimetry in low-Earth orbit and beyond." Nuclear Instruments and Methods in Physics Research Section B: Beam Interactions with Materials and Atoms 184.1 (2001): 255-294.

[15] Hassler, Donald M., et al. "Mars' surface radiation environment measured with the Mars Science Laboratory's Curiosity rover." science 343.6169 (2014): 1244797.

[16] Berger, Thomas. "Radiation dosimetry onboard the international space station ISS." Zeitschrift für medizinische Physik 18.4 (2008): 265-275.

[17] www.nasa.gov/mission_pages/station/research/news/3Draratchet_wrench

[18] ASTM D638-14, Standard Test Method for Tensile Properties of Plastics, ASTM International, West Conshohocken, PA, 2014, www.astm.org.

[19] ASTM D790-15e2, Standard Test Methods for Flexural Properties of Unreinforced and Reinforced Plastics and Electrical Insulating Materials, ASTM International, West Conshohocken, PA, 2015, www.astm.org.

[20] ASTM D3039 / D3039M-14, Standard Test Method for Tensile Properties of Polymer Matrix Composite Materials, ASTM International, West Conshohocken, PA, 2014, www.astm.org.

[21] ASTM D2240-15, Standard Test Method for Rubber Property—Durometer Hardness, ASTM International, West Conshohocken, PA, 2015, www.astm.org.

[22] Tymrak, B. M., M. Kreiger, and Joshua M. Pearce. "Mechanical properties of components fabricated with open-source 3-D printers under realistic environmental conditions." Materials & Design 58 (2014): 242-246.

[23] Torrado, Angel R., and David A. Roberson. "Failure Analysis and Anisotropy Evaluation of 3D-Printed Tensile Test Specimens of Different Geometries and Print Raster Patterns." Journal of Failure Analysis and Prevention: 1-11.

[24] Croccolo, Dario, Massimiliano De Agostinis, and Giorgio Olmi. "Experimental characterization and analytical modelling of the mechanical behaviour of fused

deposition processed parts made of ABS-M30." Computational Materials Science 79 (2013): 506-518.

[25] Bellini, Anna, and Selçuk Güçeri. "Mechanical characterization of parts fabricated using fused deposition modeling." Rapid Prototyping Journal 9.4 (2003): 252-264.

[26] Rankouhi B, Javadpour S, Delfanian F, Letcher T. "Failure Analysis and Mechanical Characterization of 3D Printed ABS With Respect to Layer Thickness and Orientation." Journal of Failure Analysis and Prevention. 2016 Jun 1;16(3):467-81.

[27] Cassidy, James, Sepehr Nesaei, Robert McTaggart, and Fereidoon Delfanian. "Mechanical response of high density polyethylene to gamma radiation from a Cobalt-60 irradiator." Polymer Testing 52 (2016): 111-116.

[28] Tekinalp, Halil L., Vlastimil Kunc, Gregorio M. Velez-Garcia, Chad E. Duty, Lonnie J. Love, Amit K. Naskar, Craig A. Blue, and Soydan Ozcan. "Highly oriented carbon fiber–polymer composites via additive manufacturing."Composites Science and Technology 105 (2014): 144-150.

APPENDIX 1

Tensile test result analysis code written in Matlab:

```
clear all
close all
clc
prompt = 'Width?\n';
W = input(prompt);
width = W*0.001;   %in meters
prompt = 'Thickness?\n';
T = input(prompt);
thickness = T*0.001;    %in meters
prompt = 'File name?\n';
N = input(prompt,'s');
filename = N;
filename2 = N(1:end-4);

area = width*thickness;  %m^2

temp = csvread(filename,7,0);

time = temp(:,1);   %sec
force = temp(:,3);   %N

stress = force/area;   %in Pa
strain = temp(:,4)/20;    %in mm/mm
strain = smooth(strain,90);
prompt = 'Beginning of the range?\n';
i = input(prompt);
prompt = 'End of the range?\n';
j = input(prompt);
range = [i:j];
[coeff] = polyfit(strain(range),stress(range),1);

E = coeff(1)

figure(1)
plot(strain,stress/1e6,strain,(E*strain+coeff(2))/1e6)
axis([0 1.1*max(strain) 0 1.1e-06*max(stress)])
xlabel('Strain (mm/mm)')
ylabel('Stress (MPa)')
saveas(gcf,filename2,'fig')
```

```
saveas(gcf,filename2,'jpeg')

paste_in_Excel = [max(stress)/1e6 max(strain)*100
max(force) E/1e6]    %output is in MPa, mm/mm, MPa
```

APPENDIX 2

Flexural test analysis code written in Matlab:

```
clear all
close all
clc

width = 0.01307;   %in m
thickness =0.00389;    %in m
span = 50e-3;   %in m
filename = '5.txt';
filename2 = '5';

area = width*thickness;  %m^2

temp = csvread(filename,7,0);

time = temp(:,2);   %sec
disp = temp(:,3)*10^-3;   %m
disp = disp-disp(1);
force = temp(:,1);   %N

stress = 3*force*span/(2*width*thickness^2);   %in Pa
strain = 6*disp*thickness/(span^2);    %in m/m
range = [30:80];
[coeff] = polyfit(strain(range),stress(range),1);

E = coeff(1);

strain_plus = stress/E + 0.002;

for i=1:length(stress)
    flip = sign(stress(i)-(E*(strain(i)-.002)+coeff(2)));
    if flip ~= 1
        break
    end
end

yield_stress = stress(i)
yield_strain = strain(i)


figure(1)
plot(strain,stress/1e6)
```

```
xlabel('Strain (mm/mm)')
ylabel('Stress (MPa)')
saveas(gcf,filename2,'fig')
saveas(gcf,filename2,'jpeg')

figure(2)
plot(strain,stress/1e6,strain,(E*strain+coeff(2))/1e6,strai
n+.002,(E*strain+coeff(2))/1e6)
xlabel('Strain (mm/mm)')
ylabel('Stress (MPa)')

paste_in_Excel = [max(stress)/1e6 yield_stress/1e6,
max(stress)/1e6 E/1e6 max(strain)*100 ]    %output is in
MPa, MPa, MPa, MPa, %
```